

AD-A141 215

THE USE OF SATELLITE OBSERVED COOD PATTERN IN
NORTHERN HEMISPHERE 300 M. (U) NAVAL ENVIRONMENTAL
PREDICTION RESEARCH FACILITY MONTEREY CA.

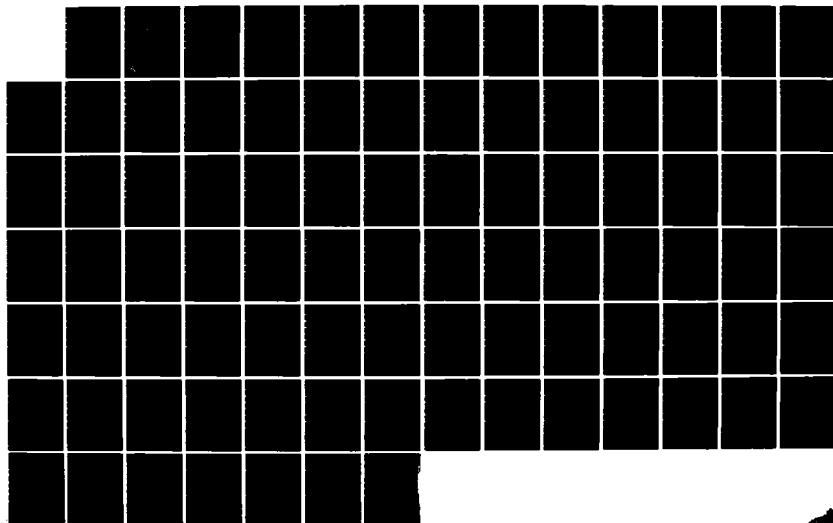
1/1

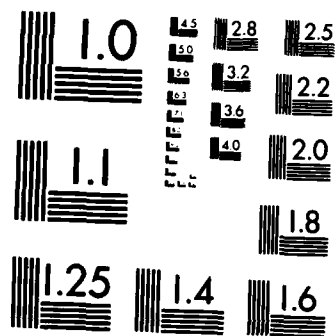
UNCLASSIFIED

FEB 84 NEPRF-TR-84-02

S D SWADLEY
F/G 4/2

NL





MICROCOPY RESOLUTION TEST CHART
NATIONAL BUREAU OF STANDARDS-1963-A



NAVENVPREDRSCHFAC
TECHNICAL REPORT
TR 84-02

NAVENVPREDRSCHFAC TR 84-02

AD-A141 215

THE USE OF SATELLITE OBSERVED CLOUD PATTERNS IN NORTHERN HEMISPHERE 300 MB AND 1000/300 MB NUMERICAL ANALYSIS

Steven D. Swadley

Naval Environmental Prediction Research Facility

FEBRUARY 1984

APPROVED FOR PUBLIC RELEASE
DISTRIBUTION UNLIMITED

DTIC FILE COPY



NAVAL ENVIRONMENTAL PREDICTION RESEARCH FACILITY

MONTEREY, CALIFORNIA 93943

84 05 16 001

QUALIFIED REQUESTORS MAY OBTAIN ADDITIONAL COPIES
FROM THE DEFENSE TECHNICAL INFORMATION CENTER.
ALL OTHERS SHOULD APPLY TO THE NATIONAL TECHNICAL
INFORMATION SERVICE.

UNCLASSIFIED

SECURITY CLASSIFICATION OF THIS PAGE (When Data Entered)

REPORT DOCUMENTATION PAGE		READ INSTRUCTIONS BEFORE COMPLETING FORM
1. REPORT NUMBER NAVENVPREDRSCHFAC Technical Report TR 84-02	2. GOVT ACCESSION NO. AD-A141 215	3. RECIPIENT'S CATALOG NUMBER
4. TITLE (and Subtitle) The Use of Satellite Observed Cloud Patterns in Northern Hemisphere 300 mb and 1000/300 mb Numerical Analysis		5. TYPE OF REPORT & PERIOD COVERED Final
7. AUTHOR(s) Steven D. Swadley		6. PERFORMING ORG. REPORT NUMBER TR 84-02
9. PERFORMING ORGANIZATION NAME AND ADDRESS Naval Environmental Prediction Research Facility Monterey, CA 93943		8. CONTRACT OR GRANT NUMBER(s)
11. CONTROLLING OFFICE NAME AND ADDRESS Naval Air Systems Command Department of the Navy Washington, DC 20361		10. PROGRAM ELEMENT, PROJECT, TASK AREA & WORK UNIT NUMBERS PE 62759N PN WF59-553 TA 1 NEPRF WU 6.2-16
14. MONITORING AGENCY NAME & ADDRESS (if different from Controlling Office)		12. REPORT DATE February 1984
		13. NUMBER OF PAGES 86
		15. SECURITY CLASS. (of this report) UNCLASSIFIED
		15a. DECLASSIFICATION/DOWNGRADING SCHEDULE
16. DISTRIBUTION STATEMENT (of this Report) Approved for public release; distribution unlimited.		
17. DISTRIBUTION STATEMENT (of the abstract entered in Block 20, if different from Report)		
18. SUPPLEMENTARY NOTES		
19. KEY WORDS (Continue on reverse side if necessary and identify by block number) Satellite data Numerical prediction Extratropical cyclones Objective analysis Bogus techniques		
20. ABSTRACT (Continue on reverse side if necessary and identify by block number) A quasi-objective statistical method for deriving 300 mb geopotential heights and 1000/300 mb thicknesses in the vicinity of extratropical cyclones with the aid of satellite imagery is presented. The technique utilizes satellite observed extratropical spiral cloud pattern parameters in conjunction with parameters derived from the original height or thickness field which has been scale separated into additive long and short wavelength component fields. Empirical relationships between extratropical spiral cloud patterns (continued on reverse)		

DD FORM 1473

JAN 73

EDITION OF 1 NOV 65 IS OBSOLETE
S/N 0102-014-6601

UNCLASSIFIED

SECURITY CLASSIFICATION OF THIS PAGE (When Data Entered)

CONTENTS

Chapter 1. Introduction	
1.1 Statement of the problem	1
1.2 Objective	2
1.3 Approach	2
Chapter 2. Background	
2.1 Satellite Data for Numerical Weather Prediction	4
2.2 Previous Studies using 500 mb Fields	5
2.3 Extension to 300 mb and 1000/300 mb Fields	7
2.4 The Scale Separation Technique	8
2.5 Significance of the Short Wavelength Component	14
Chapter 3. Data and Analysis	
3.1 300 mb and 1000/300 mb Field Data	17
3.2 The Satellite Data	19
3.3 Satellite Analysis Scheme	20
3.4 Statisitcal Methodology	26
Chapter 4. Results	
4.1 300 mb Dependent Data Set	30
4.2 1000/300 mb Dependent Data Set	35
Chapter 5. Verification of Technique	
5.1 300 mb Independent Data Set	44
5.2 1000/300 mb Independent Data Set	44
Chapter 6. Conclusions and Recommendations	
6.1 Conclusions	50
6.2 Recommendations for Future Study	52

CONTENTS (Continued)

Appendix A Further Properties of the Scale Separation Technique	54
Appendix B Development of Statistical Methodology	65
Appendix C Operational Application	73
References	78
Acknowledgments	81
Distribution	82

CHAPTER 1

Introduction

1.1 Statement of the Problem

When the first satellite images of the earth appeared in the early 1960's, it was apparent that cloud patterns associated with extratropical wave cyclones have remarkable similarities during comparable stages of development. Proper interpretation of these cloud patterns allow the location of frontal zones and vorticity centers, as well as, the stage of storm development to be determined. Furthermore these patterns agreed extremely well with the classical models of clouds and weather associated with wave cyclone life cycles.

Although synoptic scale cloud patterns over the entire globe have been monitored daily by meteorological satellites, their use in numerical weather analysis has been limited by the difficult task of making quantitative inference about the mass structure of the atmosphere from cloud field data (Broderick, 1969). Prerequisite to the use of satellite observed cloud field data in numerical weather analysis is the establishment of consistent relationships between cloud patterns and parameters which are readily transformable into data suitable for a numerical analysis scheme.

1.2 Objective

The primary purpose of the present study is to formulate an objective statistical technique to derive 300 mb geopotential heights and 1000/300 mb thicknesses from a combination of satellite observed extratropical spiral cloud patterns and parameters computed from the initial height and thickness fields.

1.3 Approach

An investigation was undertaken to establish the statistical relationship between the negative geopotential extrema associated with short (synoptic scale) wave disturbances and parameters derived from satellite observed spiral cloud patterns and the planetary scale long wave (smoothed) geopotential field.

The approach to the problem consisted of the following steps:

- i) a detailed review of previous studies to aid in developing methodology,
- ii) development of methodology and satellite analysis scheme based upon past studies and present technology and,
- iii) development and verification of the multiple linear regression equations for estimating the magnitude of the negative extrema in the height and thickness fields.

Results of items (i)-(iii) will then be used in designing the practical details for applying these techniques in an operational mode utilizing a man-machine interactive computer display system.

Chapter 2

Background

2.1 Satellite Data for Numerical Weather Prediction

During the first decade of satellite meteorology (1960-70), the operational value of satellite imagery in synoptic analysis was demonstrated. In the same period, weather forecasting was moving into the age of numerical prediction where the impact of satellite imagery was limited due to the difficulty of converting imagery into information useful to numerical analysis (Bizzari, 1982). Thus, the use of satellite imagery has been limited primarily to short range forecasting.

The second and third decades of satellite meteorology have seen considerable efforts in the development of technologies and techniques for providing quantitative satellite-derived data for numerical weather prediction models. For example, the input of satellite-derived vertical temperature profiles and cloud tracked winds in numerical prediction models have had a positive impact on numerical forecasts (Halem, et al, 1977; Seaman and Hayden, 1979; and Tracton, 1977). One of the problems of this quantification is that the satellite data tend to reduce the amplitudes of the synoptic systems (i.e. versus those depicted by radiosonde data alone, Miller and Hayden, 1978).

2.2 Previous Studies Using 500 mb Fields

The input of satellite data into numerical analysis of the mass field based upon qualitative information from the cloud field has been limited to date by the difficulty in establishing consistent relationships between the mass and cloud fields. Previous studies relevant to this problem have dealt predominantly with the 500 mb level. This was the primary level for upper level analyses during the early years of satellite meteorology and provided the most complete upper level analysis to establish consistent relationships with the satellite observed cloud field.

Early approaches to this problem (McClain, Broderick and Ruzecki, 1965; and Bradley, Hayden and Wiin-Nielsen, 1966) made use of the approximate relationship between the vorticity advection term in the quasi-geostrophic "omega equation" and vertical motions at the 500 mb level associated with the satellite observed cloud features. When a given synoptic situation was reanalyzed, the Laplacian of the stream function field was then altered in the region influenced by the satellite observed cloud system and then melded into the initial Laplacian field neighboring the region. The result of modifying the Laplacians of the stream function field at 500 mb based upon satellite imagery is not known until the actual stream function field is retrieved by solving a Poisson equation. A problem with this method is that the final stream function field can show

modifications outside the region of influence defined by the cloud features. These modifications are a computational result of the scheme used to numerically integrate the Poisson equation.

Nagle and Hayden (1971) developed a quasi-objective technique to modify the 500 mb short wavelength component field as opposed to modifying the Laplacian of the stream function field. The short wavelength component field is derived via a scale separation process in which the geopotential field is separated into additive short and long wavelength component fields, i.e. a spatial mean flow and superimposed disturbances (Holl, 1963). The scale separation method does not require the numerical integration of the Poisson equation and avoids the problems associated with the region of influence because of the additive properties of the long and short wavelength fields.

Nagle and Hayden developed regression equations from which the magnitude of the negative extrema in the 500 mb short wavelength component field can be computed as a function of parameters derived from satellite observed spiral cloud geometry and the long wavelength component of the 500 mb geopotential field. A critical assumption in the technique is that the long wavelength component of the 500 mb geopotential field can be accurately resolved by the current observational network.

Results indicate that the magnitude of the negative

extrema in the short wavelength component field can be specified with a proper interpretation of the spiral cloud features. Furthermore, the resulting modified 500 mb height field can improve the numerical analysis in data sparse regions.

2.3 Extension to 300 mb and 1000/300 mb Fields

Recently, increased emphasis is being placed upon the 300 mb level as the primary level for upper air analysis. This is a result of the numerous commercial and military aircraft which routinely report wind data at flight level (near 300 mb) with the aid of onboard inertial guidance systems. These data often provide a large proportion of the real data over the oceanic basins for use in the numerical analysis.

Well developed extratropical cyclones viewed by satellites are depicted as broad scale spiral shaped cloud patterns in which there are cirriform clouds that are closely linked to the flow pattern near the jet stream, i.e. near 300 mb. Therefore, the extension of the previous work to the 300 mb level is physically sound.

One of the problems with inserting bogus height data at a single level of a multi-level numerical forecast model is that of maintaining vertical consistency among the various levels. It is well known that the typically deep, large scale vertical motions associated with major extratropical

cyclones can be partitioned between two major forcing functions: The vertical variation of vorticity advection and the Laplacian of thickness advection (Barr, Lawrence and Sanders, 1966; and Krishnamurti, 1966). Therefore, the satellite viewed extratropical cyclone is reflective of the flow pattern within a deep layer of the atmosphere. It is for these reasons that the extension of the previous work to the 1000/300 mb layer was attempted.

2.4 The Scale Separation Technique

The scale separation technique developed by Holl (1963), as an objective version of Fjortoft's (1952) manual technique, provides a fundamental representation of the subject fields by a superposition of specific elemental fields which represent indigenous patterns. Holl defined a new representation of the spectrum of a field and developed a technique for decomposing the field into additive component fields.

The technique successively applies a smoothing operator to the subject field until the amplitude of a specified wavelength component is reduced to some percentage of its initial value, say five percent. Appendix A contains a detailed discussion of the smoothing process. Since the smoothing operator is linear, all subsequent additions and subtractions yielding components of the original field are commutative.

The smoothing filter as defined by Holl is given by:

$$Z_{LW} = Z_0 + C \int_0^\alpha \nabla^2 Z \, d\alpha = Z_0 - Z_{sw} \quad (1)$$

where Z_{LW} is the long wavelength field, Z_0 is the original field, Z_{sw} is the short wavelength field, C is a constant, and α is the smoothing parameter.

Holl originally developed this technique for use with the Northern Hemisphere Polar Stereographic grid configuration. There are 63 x 63 grid points for a total of 3969 points. The grid distance is 381 km, true at 60° N. The map factor for the grid is:

$$m_{ij} = \frac{1 + \sin 60^\circ}{1 + \sin \phi_{ij}} \quad , \quad (2)$$

where ϕ_{ij} is the latitude at grid point i, j . This grid configuration was used for the present study. The degree of smoothing used for this study was $\alpha = 5.0$.

The amplitude reduction factor as a function of wavelength (in grid lengths) is given in Figure 1. The response curve is that for first order smoothing. Since it is desirable to have a much steeper response curve, third order smoothing, as explained in Appendix A, was used for this study.

Examples of the scale separation technique applied to a 300 mb height field are shown in Figures 2, 3 and 4. Figure 2 is the initial height field; Figure 3 is the long wavelength field resulting from the smoothing process. The

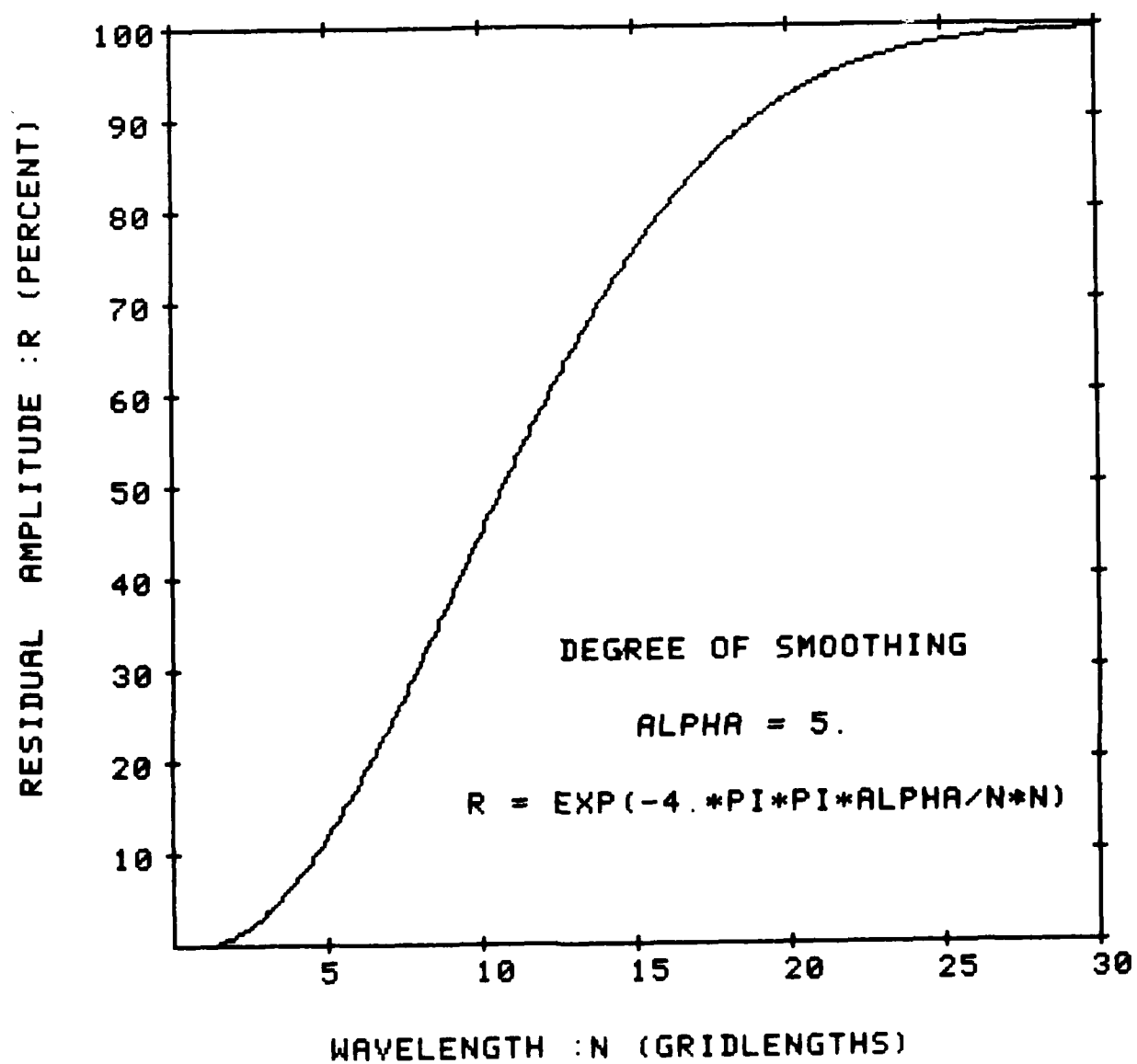


Figure 1. Amplitude reduction factor as a function of wavelength (in grid lengths).

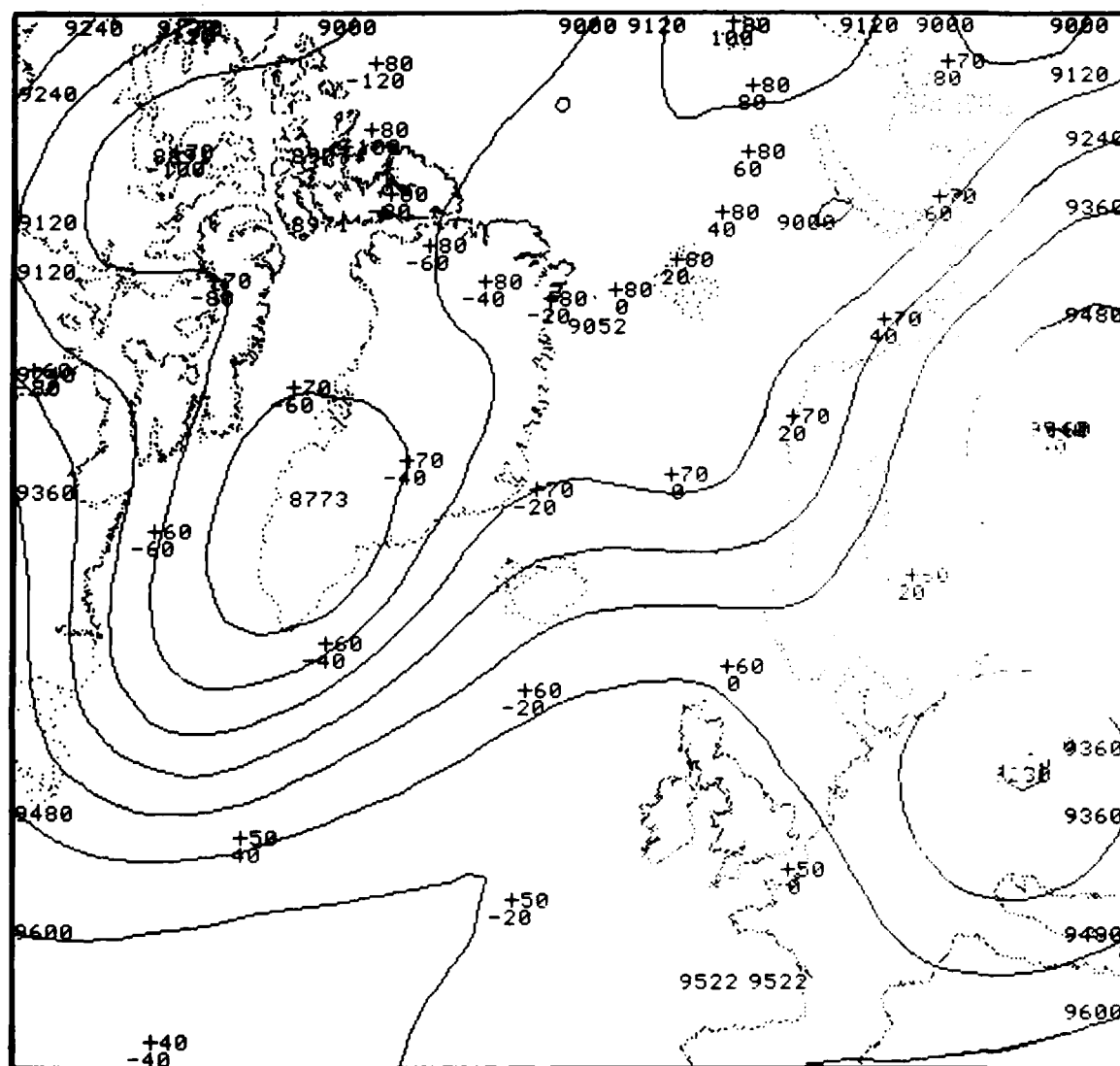


Figure 2. Initial 300 mb height field, 1200 GMT, August 5, 1983.

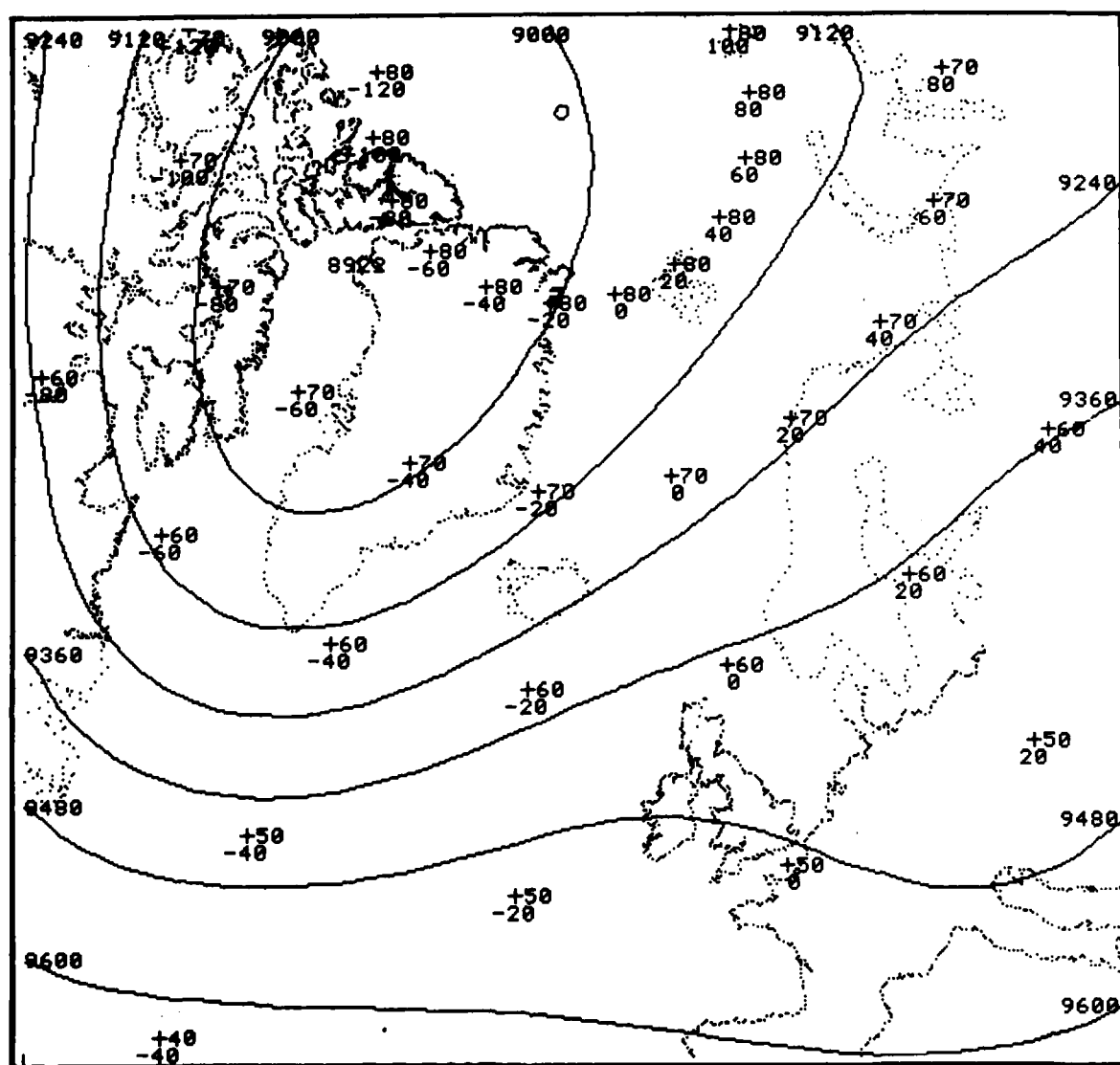


Figure 3. 300 mb long wavelength (SR) component field, 1200 GMT, August 5, 1983.

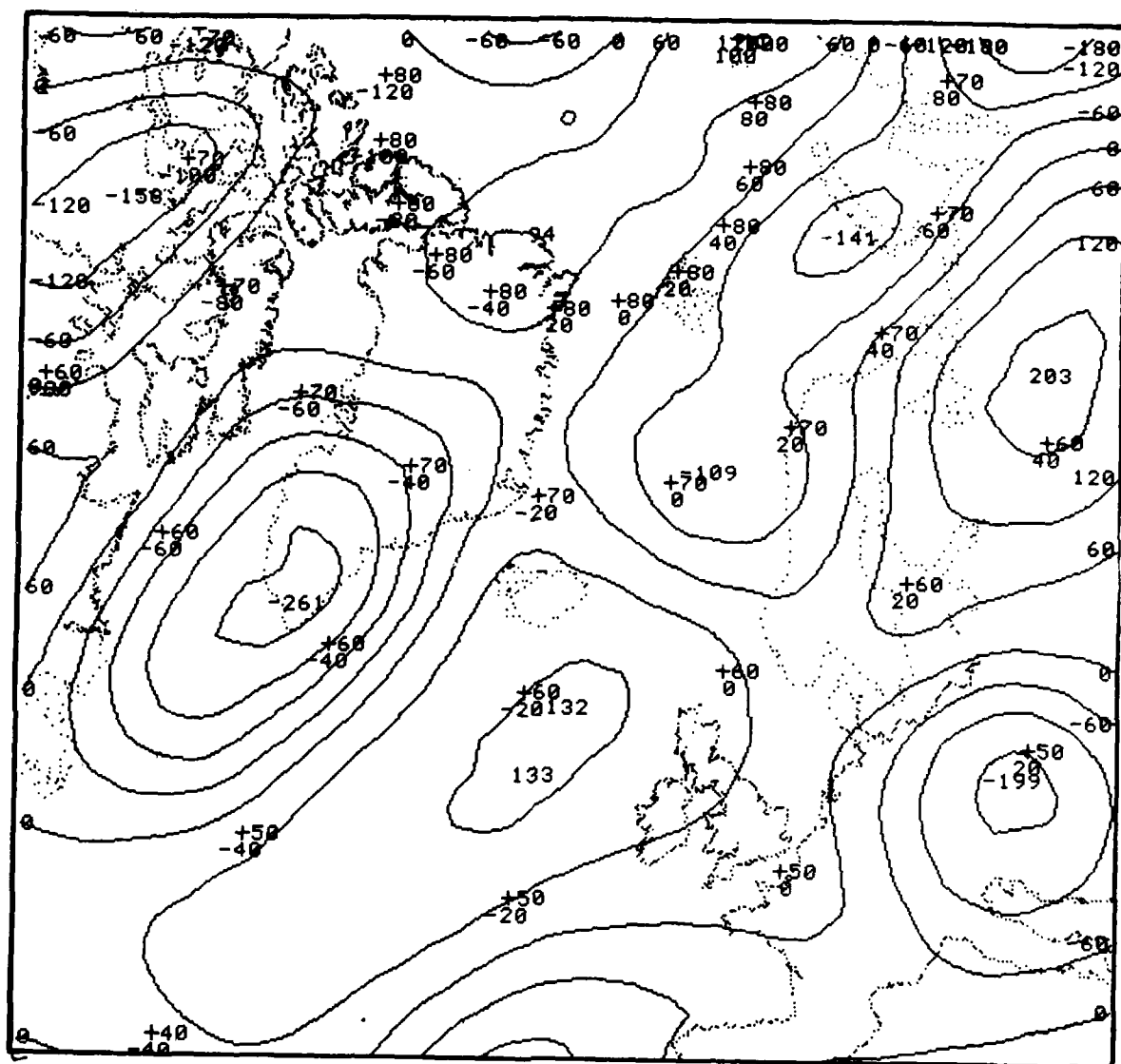


Figure 4. 300 mb short wavelength (SD) component field, 1200 GMT, August 5, 1983.

short wavelength field is constructed by subtracting the long wavelength field from the initial field and is shown in Figure 4.

2.5 Significance of the Short Wavelength Component

The short wavelength component field is significant because it closely resembles the relative vorticity field (Nagle, et al., 1966). The spiral cloud systems are related to the short wave systems moving through larger scale patterns (Whitney and Herman, 1968). Thus, satellite observed spiral cloud pattern geometry can be used to modify the short wavelength component field. The adjusted short wavelength field is then added to the long wavelength field to yield the modified total height field.

The short wavelength component defined in (1) is given by:

$$Z_{sw} = -c \int_0^{\alpha} \nabla^2 Z \, d\alpha. \quad (3)$$

From the calculus, the mean value theorem for integrals states that, if $\nabla^2 Z$ is continuous over the interval $[0, \alpha]$, then there exists a value α^* , where $0 < \alpha^* < \alpha$, such that

$$Z_{sw} = -c \, \alpha \nabla^2 Z(\alpha^*), \quad (4)$$

where $Z(\alpha^*)$ represents the partially smoothed field at the

degree of smoothing, α^* .

The geostrophic relative vorticity, ζ_g , is given by

$$\zeta_g = gf^{-1} \nabla^2 Z, \quad (5)$$

where g is gravity and f the coriolis parameter. Therefore, the relationship between the geostrophic relative vorticity and the short wavelength component depends upon the latitude and the equality of $\nabla^2 Z(\alpha^*)$ and $\nabla^2 Z_0$. A direct proportionality between the magnitudes of these fields cannot be expected because of the wavelength dependence of the Laplacian operator, although the patterns of the $\nabla^2 Z(\alpha^*)$ and ζ_g fields should be remarkably similar. The locations of the field extrema and/or zero values should also be similar (see Figures 4 and 5).

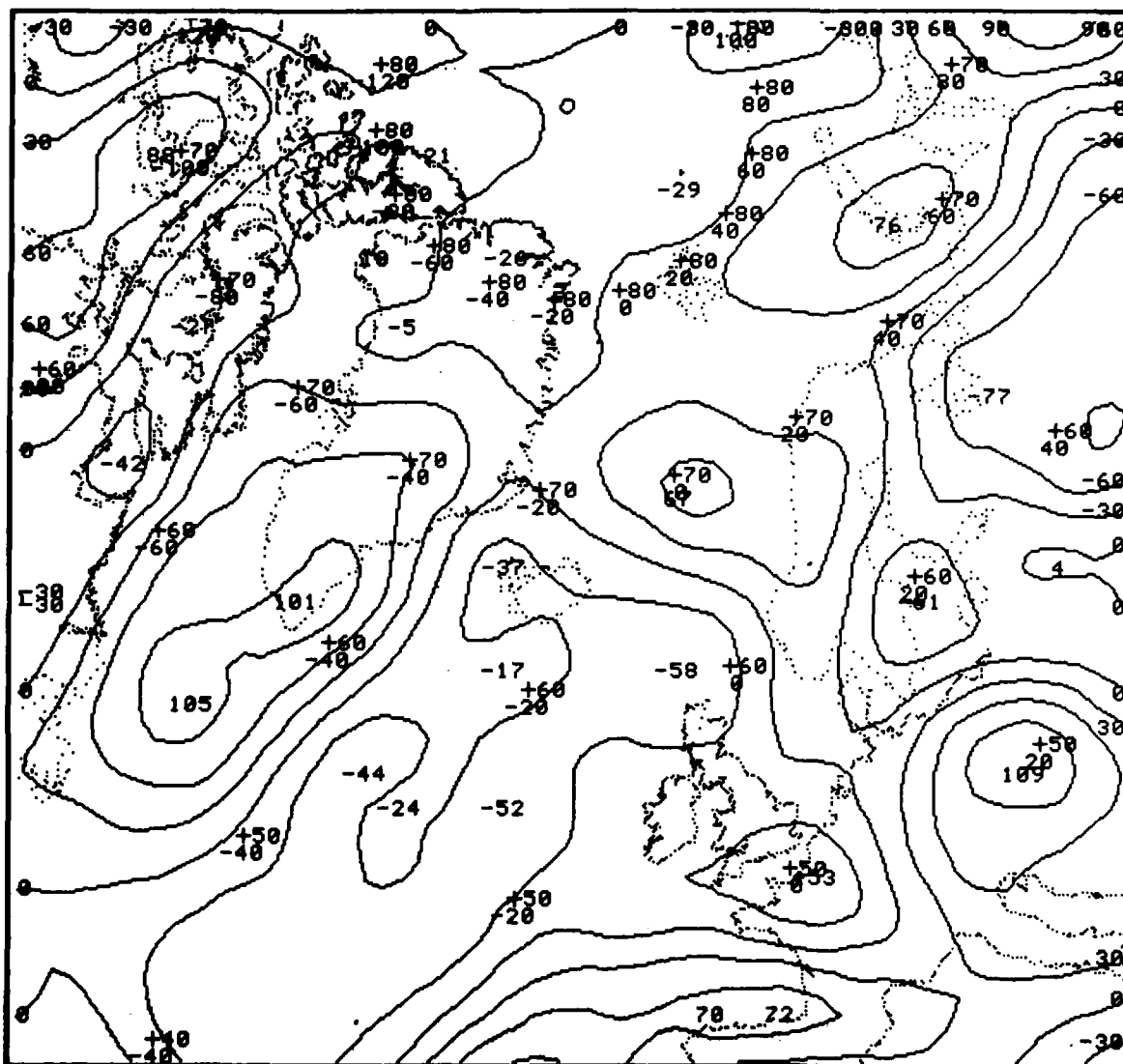


Figure 5. 300 mb relative vorticity field, 1200 GMT, August 5, 1983.

Chapter 3

Data and Analysis

3.1 300 mb and 1000/300 mb Field Data

The field data were provided by the U.S. Navy's Fleet Numerical Oceanography Center (FNOC). The height and thickness values were available on the polar stereographic (63 x 63) grid points. The scale separation technique was applied, with $\alpha = 5$, to generate the short wavelength (SD) field and the residual (SR) field. The planetary vortex (SV) field is obtained by applying the scale separation technique with $\alpha = 16.5$ which acts as an extreme low pass filter. The long wavelength (SL) field is then determined using the following relationship with the original field Z,

$$Z = SR + SD = SV + SL + SD. \quad (6)$$

The SR field is usually considered the long wave field (see Figure 3) but is actually the sum of the SV and SL fields computed by the scale separation technique. The 300 mb SV field corresponding to Figure 2, 3 and 4 is shown in Figure 6.

The following parameters were computed at the centers of the significant SD field extrema: The latitude and longitude, the height value, the u and v geostrophic

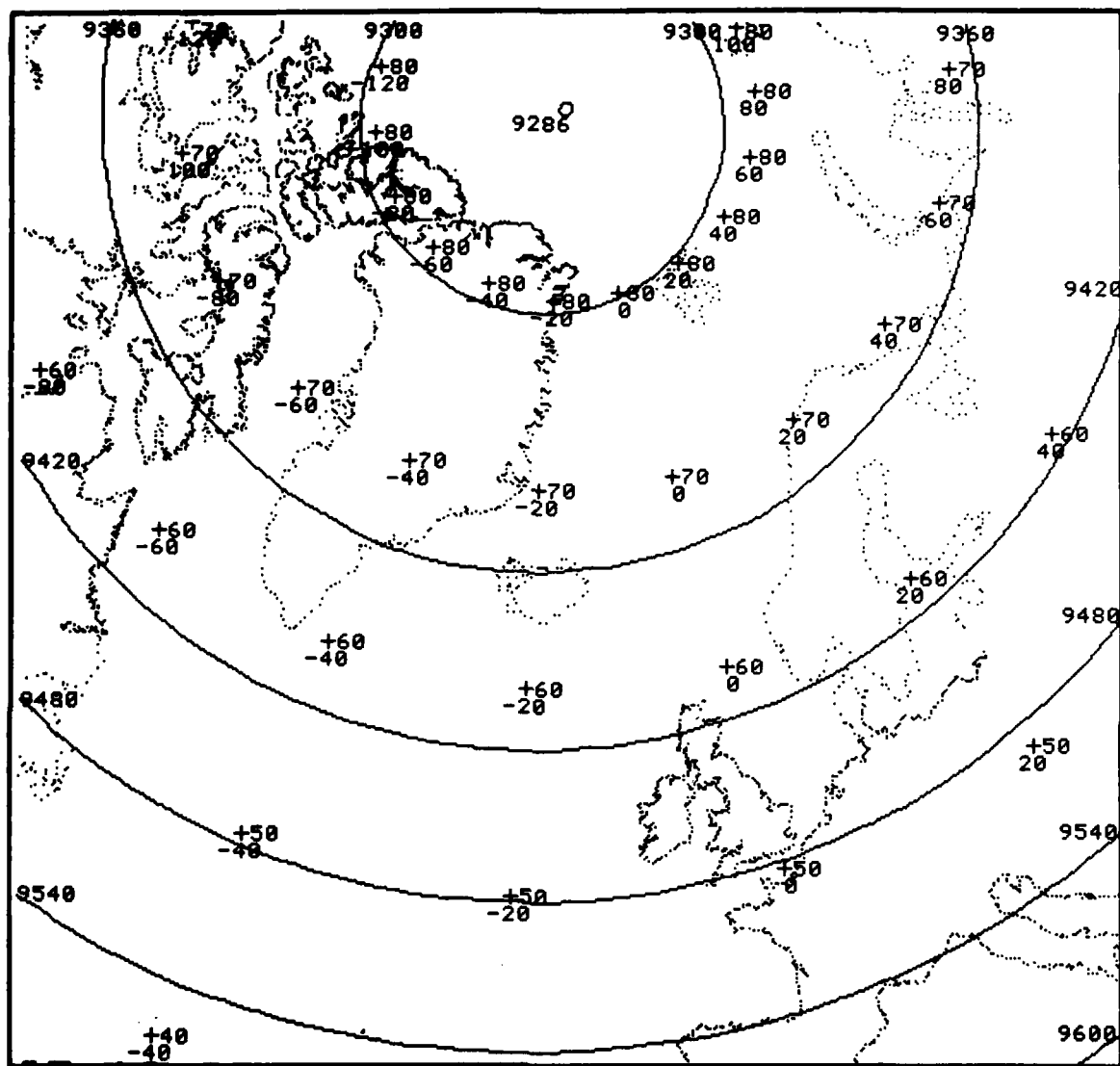


Figure 6. 300 mb planetary vortex (SV) field,
1200 GMT, August 5, 1983.

velocity components and the Laplacian using a five-point finite difference stencil. These parameters were computed for the SR, SV and SL component fields of the original 300 mb height and 1000/300 mb thickness fields. The data set consists of the above parameters computed for both the 1200 GMT analysis and the 12 hour forecast from the previous 0000 GMT forecast. The data was collected on a daily basis for the time period 29 August, 1981, to 19 September, 1982. Plots of both the 300 mb height and 1000/300 mb thickness SD fields for the 1200 GMT analysis were also collected.

3.2 The Satellite Data

The satellite data used for this study was acquired by the NOAA-7, which was the second operational satellite in the TIROS-N series. Launched on 23 June, 1981, the NOAA-7 satellite is a sun-synchronous (polar-orbiting) meteorological satellite with an orbital altitude of 850 km and a travel speed of about 6.6 km/sec. The NOAA-7 Advanced Very High Resolution Radiometer (AVHRR) is a five channel instrument: two channels in the visible and near infrared (IR), 0.58 - 0.68 μm and 0.725 - 1.10 μm ; one in the IR window region at 4 μm , 3.55 - 3.93 μm and two in the thermal IR window at 11 μm , 10.5 - 11.3 μm and 11.5 - 12.5 μm . The imagery used for this study was from the visible, near IR, and thermal IR. The images used were Northern Hemisphere Polar Stereographic mosaics composed of successive satellite

passes over the North Atlantic ranging in time from 1300 - 2000 GMT. The satellite imagery was available for the same period as the field data collection period with the exception of the entire month of March 1982. The images for March were not available and thus not included in this study.

3.3 Satellite Analysis Scheme

The well documented correspondence between specific satellite observed spiral cloud features and synoptic features associated with upper-tropospheric relative vorticity fields was summarized by Nagle and Hayden as follows:

- 1) The boundaries of cellular convective cloud areas and the trailing edges of frontal cloud bands correspond to the zero line in the relative vorticity field.
- 2) The locations of extratropical spiral cloud centers associated with cold-core systems correspond to positive vorticity maxima.
- 3) The leading edges of frontal cloud bands correspond to axes of maximum of negative relative vorticity.
- 4) The apex of the anticyclonic curvature of the leading edges of frontal cloud bands correspond to the negative relative vorticity maxima.

These relationships permit a rather complete specification of the pattern of the short wavelength

component field provided a proper interpretation of the spiral cloud pattern is made. The magnitude of the negative extrema in the short wavelength component (SD) field remains to be specified.

The spiral cloud patterns were analyzed as follows. A quarter hemisphere polar stereographic NOAA-7 mosaic (preferably IR) of the North Atlantic covering from 10° E to 80° W longitude was selected corresponding to the date of the field data. The 300 mb and 1000/300 mb SD field plots were compared with the satellite image to identify the spiral cloud systems with significant and distinct negative extrema in the SD field. If a spiral system was evident without the presence of a distinct SD feature, the SD field was considered in error and the analysis was discontinued for that date. This was an effective gross error checking procedure which prevents spurious parameters from entering the statistical analysis.

The latitude and longitude of the center of a spiral cloud pattern was recorded as SLAT and SLON to the nearest whole degree. The latitude and longitude of the center of the SD extrema as computed by the scale separation technique program was recorded as FLAT and FLON. These would later be used as identifiers in searching the field data file to extract the other computed parameters for that SD feature. Since the satellite images are mosaics composed of successive NOAA-7 orbits ranging from 1300 to 2000 GMT, a systematic

spatial and temporal error is evident. The difference between SLAT, SLON and FLAT, FLON are summarized in Tables 1 and 2 for the 300 mb and 1000/300 mb SD fields respectively. These errors are also partially attributed to errors in the original analysis.

The location of the upper-tropospheric trough (i.e., where the high clouds abruptly end or have a distinguishable gap along the major frontal cloud band) is then determined. A line is then drawn from the spiral center to the point where the upper-tropospheric trough intersects the outer edge of the frontal band. This distance is defined as the amplitude (AMP) of the satellite observed cloud system.

A line is now drawn perpendicular to the line defining the amplitude and passing through the spiral center. The intersections of this line with the westernmost and easternmost edges of the spiral cloud band define the wavelength (RL) of the satellite observed cloud system. In actuality this is a half-wavelength when considering the ridge-trough system as the full wavelength.

All distances are defined in terms of gridlengths (381 km at 60° N). The schematic representation of the above analysis procedure for an idealized spiral cloud system is shown in Figure 7.

The final subjective assessment about the spiral cloud system is the stage of development parameter (IST). A modified version of McClain and Broderick's (1967) stage of

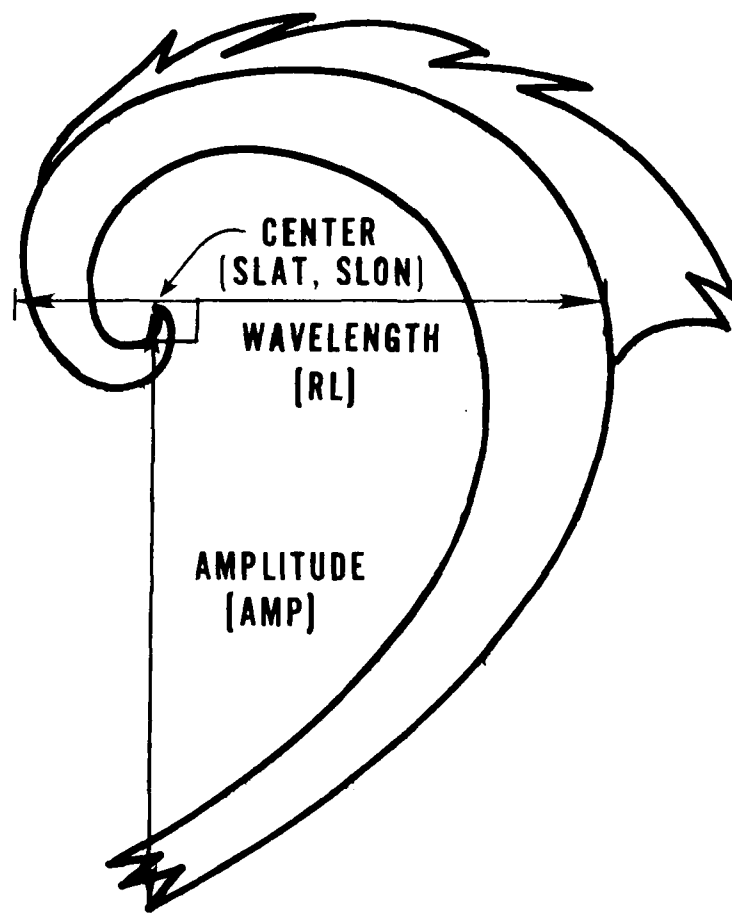


Figure 7. Idealized spiral cloud system.

development classification system was used. Figure 8 shows the various stages of development used for the study. The stage of development parameter along with SLAT, SLON, AMP and RL were obtained for each spiral cloud system that could be associated with a specific minimum in the SD field. The total number of cases analyzed in the above manner is 421 for the 300 mb height field cases and 420 1000/300 mb thickness field cases.

3.4 Statistical Methodology

A regression equation of the form

$$y = b_1x_1 + b_2x_2 + \dots + b_nx_n = \sum_{j=1}^n b_jx_j \quad (7)$$

is used to apply the previously discussed parameters to the problem of specifying the negative SD field extrema. The special case for which x_1 is identically one, is specified, which means that b_1 now plays the role of the regression constant or y-intercept. Symbols are defined as follows:

- y = negative SD field extrema,
- b_1 = regression constant,
- b_j = regression coefficients, and
- x_j = potential predictors to be screened
($j=2,3,\dots,n$).

The stepwise multiple linear regression procedure used in the current study was the Biomedical Computer Programs P-

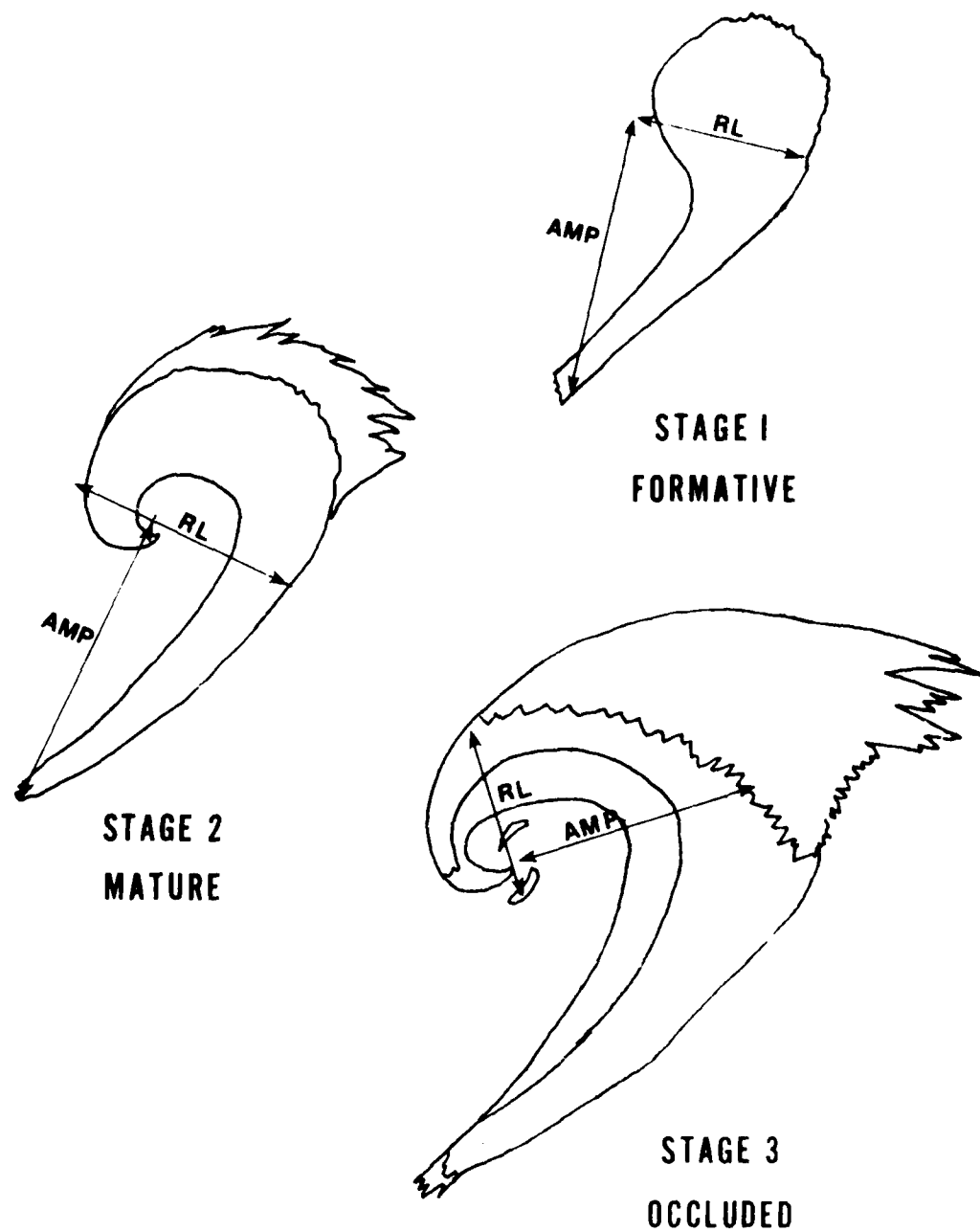


Figure 8. Schematic representation of the stage of development parameter.

series program P2R developed at the Health Science Computing Facility of the University of California at Los Angeles. A detailed discussion of the multiple regression technique and program P2R are given in Appendix C.

The data set compiled during the satellite analysis procedure had to be matched with the 300 mb and 1000/300 mb SD data sets containing the various long wave parameters. The latitude and longitude of the SD extrema (FLAT, FLON) was used to search the SD data file which also contained FLAT, FLON. To avoid minor differences due to FLAT, FLON being listed as accurate only to 1/10 of a degree, a one degree by one degree latitude and longitude box was used to provide some leeway in the searching routine.

The 300 mb and 1000/300 mb data sets were now complete. The 300 mb data set contained 413 cases while the 1000/300 mb data set contained 373 cases, each with the date time group, the observed SD value, satellite parameters and the long wave parameters. The data sets were now randomly split into dependent and independent sets. The 300 mb and 1000/300 mb dependent data sets contained 290 and 263 cases, respectively while the independent data sets contained 123 and 115 cases, respectively.

When analyzing the spiral cloud systems it became apparent that the relationship between the wavelength (RL) and the SD value behaved in a non-linear fashion. Based upon heuristic reasoning, the following variables with non-

linear characteristics were added: $RL * \sin(SLAT)$, \sqrt{RL} , $RL/\cos(SLAT)$ and $RL * \sin(SLAT)$. Ratios of the amplitude and wavelength were also added as suggested by Lowe (1983). A complete list of the variables used is given in Table 3.

The program P2R was then used to process the dependent data sets. The variables were entered or removed from the regression model based upon the F method (see Appendix B). The F-to-enter and F-to-remove limits used for this study are 4.0 and 3.9, respectively with a tolerance of 0.05.

Regression runs were also performed for 300 mb and 1000/300 mb data sets without the inclusion of the satellite observed spiral cloud parameters. This was an effective check to see if there was adequate information contained in the computed long wave parameters to accurately specify the magnitude of the negative SD extrema.

TABLE 3.

3. POTENTIAL PREDICTORS

FLAT	LATITUDE OF THE SD EXTREMA
FLON	LONGITUDE OF THE SD EXTREMA
SLAT	LATITUDE OF THE CENTER OF THE SATELLITE OBSERVED CLOUD SYSTEM
SLOM	LONGITUDE OF THE CENTER OF THE SATELLITE OBSERVED CLOUD SYSTEM
AMP	AMPLITUDE OF THE SATELLITE OBSERVED CLOUD SYSTEM
RL	WAVELENGTH OF THE SATELLITE OBSERVED CLOUD SYSTEM
IST	STAGE OF DEVELOPMENT : 1 - FORMATIVE, 2 - MATURE, 3 - OCCLUDED
SRU	U-COMPONENT OF THE GEOSTROPHIC WIND DERIVED FROM THE SR FIELD AT FLAT,FLON
SRV	V-COMPONENT OF THE GEOSTROPHIC WIND DERIVED FROM THE SR FIELD AT FLAT,FLON
SLH	GEOPOTENTIAL HEIGHT OF THE SL FIELD AT FLAT,FLON
SLU	U-COMPONENT OF THE GEOSTROPHIC WIND DERIVED FROM THE SL FIELD AT FLAT,FLON
SLV	V-COMPONENT OF THE GEOSTROPHIC WIND DERIVED FROM THE SL FIELD AT FLAT,FLON
SLL	FIVE-POINT FINITE DIFFERENCE APPROXIMATION FOR THE LAPLACIAN OF THE SL FIELD AT FLAT,FLON
SVH	GEOPOTENTIAL HEIGHT OF THE SV FIELD AT FLAT,FLON
SVU	U-COMPONENT OF THE GEOSTROPHIC WIND DERIVED FROM THE SV FIELD AT FLAT,FLON
SVV	V-COMPONENT OF THE GEOSTROPHIC WIND DERIVED FROM THE SV FIELD AT FLAT,FLON
SVL	FIVE-POINT FINITE DIFFERENCE APPROXIMATION FOR THE LAPLACIAN OF THE SV FIELD AT FLAT,FLON
RLS	$RL \cdot \sin(SLAT)$
RLB	\sqrt{RL}
RLMA	$RL \cdot AMP$
AMDR	AMP/RL
RLDA	RL/AMP
RLDC	$RL/\cos(SLAT)$
RLS2	$RL \cdot \sin(SLAT) \cdot \sin(SLAT)$

Chapter 4

Results

4.1 300 mb Dependent Data Set

The basic statistical properties of the variables included in the 290 cases comprising the 300 mb dependent data set are shown in Table 4.

The following predictors were selected for use in the regression model: The square root of the system wavelength (RL5); the Laplacian of the SL field (SLL); the height of the SL field (SLH); the Laplacian of the SV field (SVL) and the U-components of the SV and SR fields (SVU and SRU). The coefficients and statistics for each independent variable in the equation as well as the multiple correlation coefficient, the squared multiple correlation coefficient, and the adjusted squared multiple correlation coefficient are shown in Table 5. The root-mean-squared (RMS) error for the observed versus predicted SD values was 30.94 meters. A plot of the residuals (observed-predicted) for this regression model is given in Figure 9. Upon examining the residual plot, it appears that the residuals fall in a horizontal band centered about the abscissa without any apparent trends, which suggests that the model may be judged as adequate (Afifi and Azen, 1979). The probable error of the correlation coefficient given by

Table 4.

300 MB : DEPENDENT DATA SET

VARIABLE	MEAN	STANDARD DEVIATION	SKEWNESS	KURTOSIS
FLAT	.82840	.15277	-.44665	.62471
FLON	.70417	.35623	.17232	-1.02394
SLAT	.84159	.15953	-.47547	.31218
SLON	.60622	.33495	.18481	-.92232
AMP	3.39130	1.27269	1.01112	1.54712
RL	2.83716	.88580	.65806	.04054
IST	2.35172	.48468	.52996	-1.47690
SD	-217.96550	53.35474	-.13033	-.04560
SRU	18.74138	8.36404	.27811	.42935
SRV	-.08276	6.18397	-.37603	.32827
SVL	3.02100	4.36309	-.87640	1.21658
SLH	-80.23103	91.74687	-.50833	.44344
SLU	5.76207	7.31710	-.38065	1.65773
SLV	-.05517	5.71722	-.42538	.36289
SLL	27.00623	18.67461	.25430	.38237
SVH	85.83102	189.75940	-.41856	-.43799
SVU	13.18621	3.20316	.43648	-.60756
SVV	.23448	.70480	.22580	1.94812
RLS	2.08902	.72151	.55330	-.18229
RL5	1.66437	.25885	.31383	-.40974
RLMA	10.52327	7.18180	1.80518	4.77913
AMOR	1.20176	.27743	1.04864	1.70518
RLDA	.87356	.19004	.51530	1.02752
RLDC	4.43903	1.56943	.84057	-.95840
RLS2	1.57011	.63935	.43046	-.18950

290 TOTAL OBSERVATIONS

TABLE 5

5. 300 mb dependent data set regression results.

Variables in Equation

VARIABLE	COEFFICIENT	STD. ERROR OF COEFF.	STD. REG. COEFF.	F-TO- REMOVE
RL5	-121.63845	8.2886	-0.590	215.37
SLL	-2.84518	0.3077	-0.996	85.50
SLH	-0.58965	0.0750	-1.014	61.82
SVL	-7.42866	0.9643	-0.607	59.35
SVU	4.73323	0.7821	0.291	36.62
SRU	-0.82807	0.3259	-0.130	6.46

INTERCEPT = -10.42469

MULTIPLE R = 0.8146

MULTIPLE R-SQUARED = 0.6637

ADJUSTED R-SQUARED = 0.6565

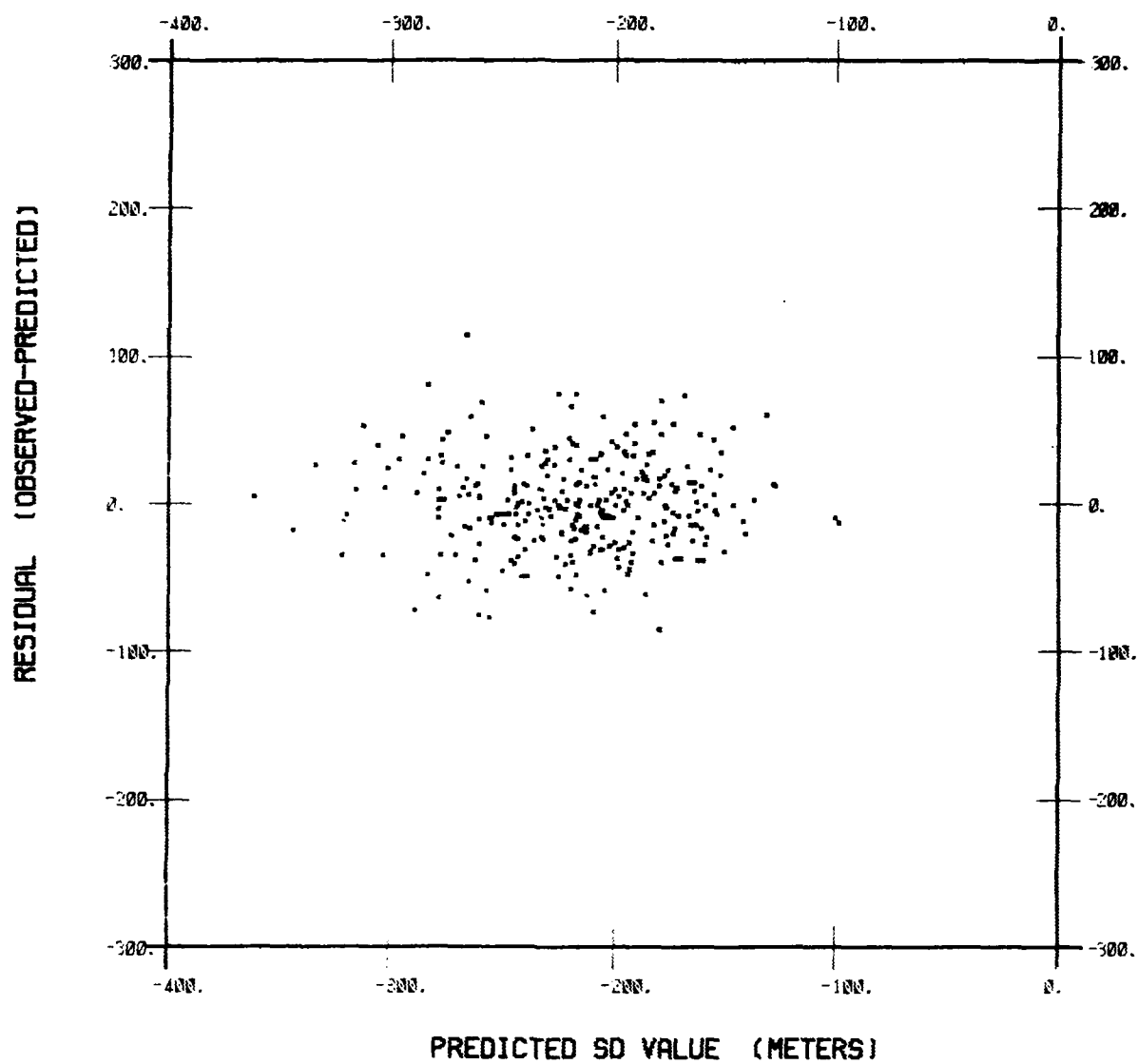


Figure 9. Scatter diagram of the predicted SD value versus the residual for the 300 mb dependent data set.

$$e = 0.6745 \frac{1-R^2}{[N]^{\frac{1}{2}}} \quad (8)$$

where R is the correlation coefficient and N the number of cases (Landsburg, 1964), is 0.013.

The following predictors were selected for the no-satellite-parameters regression model: The Laplacian of the SL field (SLL); the height of the SL field (SLH); the U-component of the SL field (SLU); the latitude of the SD extrema (FLAT) and the Laplacian of the SV field (SVL). Table 6 summarizes the regression results in the same format as Table 5. The RMS error for the observed versus predicted was 40.93 meters. A plot of the residuals for this regression model is given in Figure 10. There are no apparent trends in the residuals, but the scatter about the zero line is large enough to consider the model inadequate. The probable error of the regression coefficient is 0.023.

4.2 1000/300 mb Dependent Data Set

The basic statistical properties of the variables included in the 263 cases comprising the 1000/300 mb dependent data set are given in Table 7.

The following predictors were selected for use in the regression model: The product of the system wavelength and sine of the system latitude (RLS); the Laplacian of the SL field (SLL); the stage of development parameter (IST); the

TABLE 6

6. 300 mb dependent data set regression results (no parameters)

Variables in Equation

VARIABLE	COEFFICIENT	STD. ERROR OF COEFF.	STD. REG. COEFF.	F-TO- REMOVE
SLL	-4.32998	0.3684	-1.515	138.14
SLH	-0.82326	0.0940	-1.416	76.64
SLU	-1.81360	0.4362	-0.249	17.28
FLAT	-142.29917	35.5345	-0.407	16.04
SVL	-5.10234	1.6776	-0.417	9.25

INTERCEPT = -23.33036

MULTIPLE R = 0.6414

MULTIPLE R-SQUARED = 0.4115

ADJUSTED R-SQUARED = 0.4011

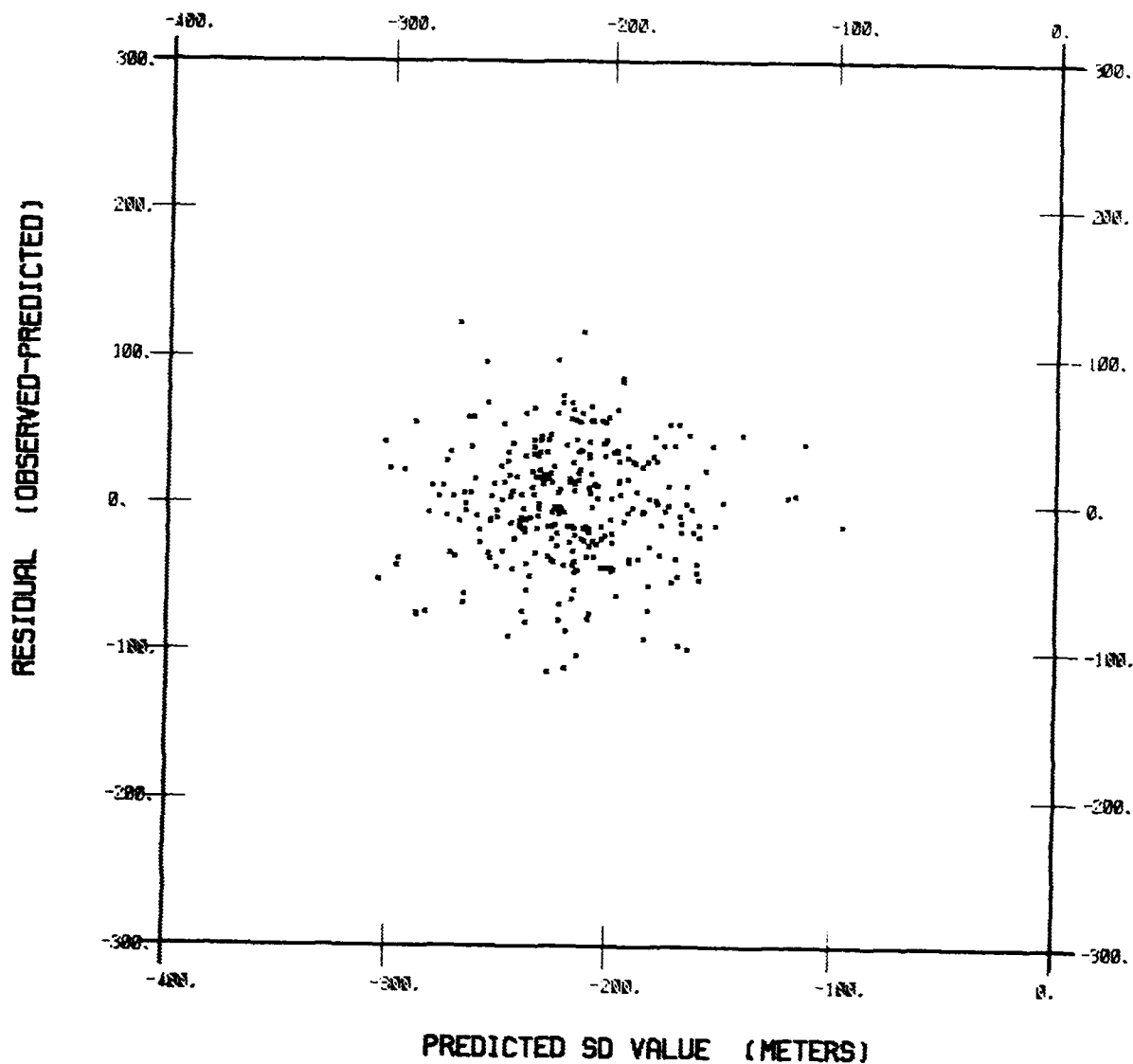


Figure 10. Scatter diagram of the predicted SD value versus the residual for the 300 mb dependent data set (no satellite parameters).

Table 7.

1000/300 MB : DEPENDENT DATA SET

VARIABLE	MEAN	STANDARD DEVIATION	SKEWNESS	KURTOSIS
FLAT	.81340	.14645	-.13985	.54160
FLON	.73611	.39217	.08333	-1.04219
SLAT	.83976	.15368	-.22732	.32350
SLON	.61395	.35139	.19790	-.74965
AMP	3.55163	1.32945	.86974	.81578
RL	2.93490	.94653	.74317	.14648
IST	2.31939	.47433	.66749	-1.26407
SD	-176.23950	55.30478	-.22924	.85936
SRU	17.23193	6.50968	.66252	.38902
SRV	-.97719	5.83091	-.91658	1.10230
SVL	3.13065	3.78742	-.59761	.67441
SLH	-50.23193	78.36052	-.68650	1.87620
SLU	4.05323	5.35694	.33100	.89081
SLV	-.82890	5.23563	-.80441	1.01086
SLL	19.76711	17.20300	.26900	1.02785
SVH	64.71863	184.98930	-.42864	-.50718
SVU	13.36882	3.19887	.06318	-.49276
SVV	.16350	.77990	-.19728	1.82237
RLS	2.15556	.75189	.71720	.16032
RL5	1.69166	.27048	.37551	-.27238
RLMA	11.46225	7.92125	1.59687	2.99606
AMDR	1.21578	.26360	.82531	1.33291
RLDA	.86041	.18481	.76750	1.60361
RLDC	4.57093	1.64756	.90890	.96800
RLS2	1.61331	.65670	.61915	.12310

263 TOTAL OBSERVATIONS

height of the SL field (SLH); the Laplacian of the SV field (SVL) and the U-components of the SV and SL fields (SVU and SLU). Table 8 summarizes the regression results in the same format as Table 5, the RMS error for the observed versus predicted was 36.02 meters. A plot of the residuals for this regression model is given in Figure 11. There are no apparent trends in the residuals, and the scatter appears acceptable, which suggests the model is adequate. The probable error of the correlation coefficient is 0.018.

The following predictors were selected for the no-satellite-parameters regression model: The heights of the SL and SV fields (SLH and SVH), and the U-component of the SR field. Table 9 summarizes the regression results in the same format as Table 5. The RMS error for the observed versus predicted was 48.51 meters. A plot of the residuals for this regression model is given in Figure 12. There are no apparent trends in the residuals, but the scatter about the zero line is large enough to consider the model inadequate. The probable error of the regression coefficient is 0.032.

TABLE 8

8. 1000/300 mb dependent dat set regression results

Variables in Equation

VARIABLE	COEFFICIENT	STD. ERROR OF COEFF.	STD. REG. COEFF.	F-TO- REMOVE
RLS	-33.62609	3.8860	-0.457	74.88
SLL	-3.22387	0.4249	-1.003	57.57
IST	38.99478	5.6850	0.334	47.05
SLH	-0.51486	0.1019	-0.729	25.52
SVU	4.07143	0.8280	0.235	24.18
SLU	-2.16366	0.5317	-0.210	16.65
SVL	-2.38556	1.1721	-0.163	4.14

INTERCEPT = -194.5239

MULTIPLE R = 0.7588

MULTIPLE R-SQUARED = 0.5758

ADJUSTED R-SQUARED = 0.5641

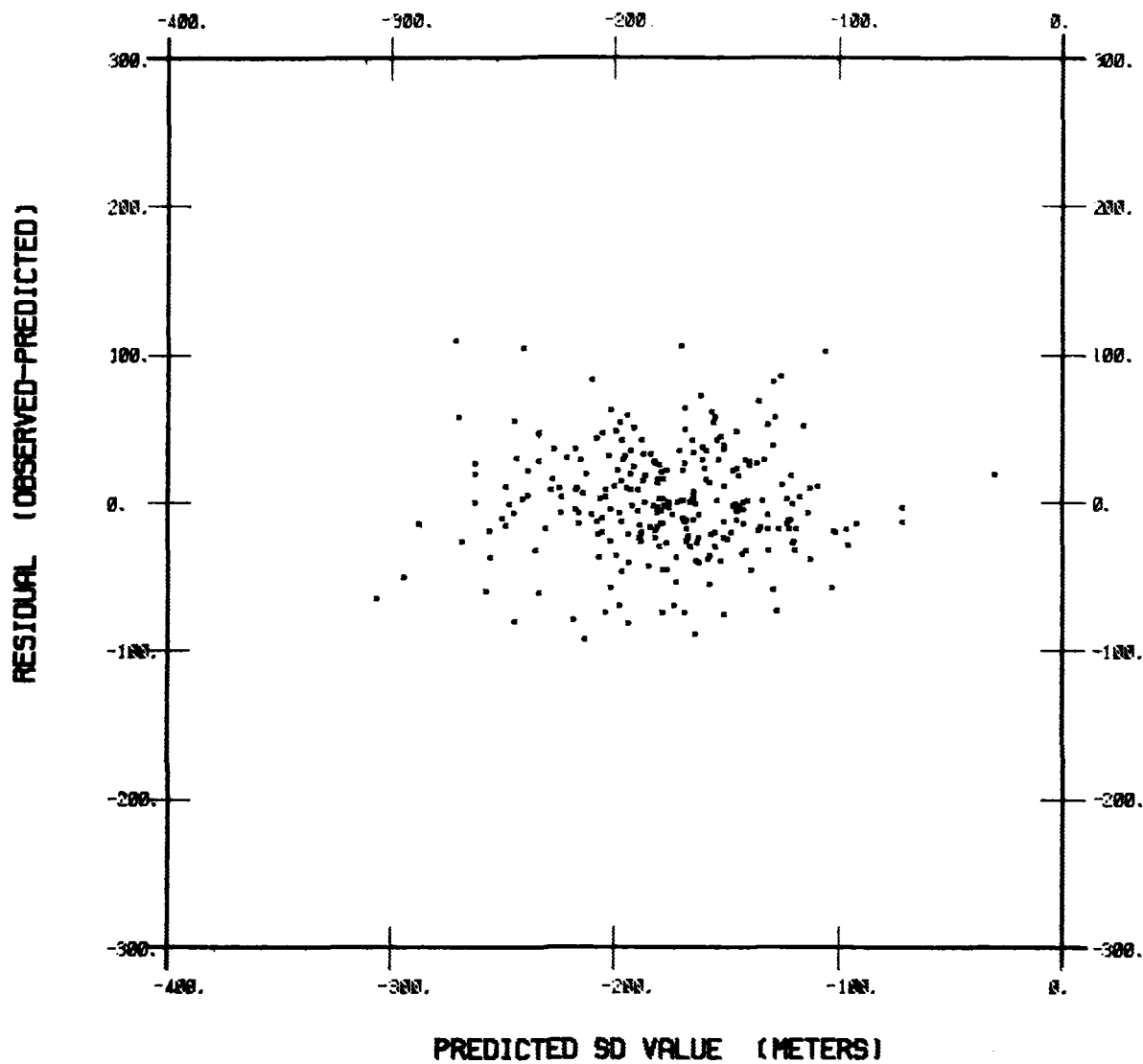


Figure 11. Scatter diagram of the predicted SD value versus the residual for the 1000/300 mb dependent data set.

TABLE 9

9. 1000/300 mb dependent data set regression results (no satellite parameters)

Variables in Equation

VARIABLE	COEFFICIENT	STD. ERROR OF COEFF.	STD. REG. COEFF.	F-TO- REMOVE
SLH	0.29457	0.0432	0.417	46.52
SVH	-0.06843	0.0177	-0.229	14.96
SRU	-1.53023	0.5198	-0.180	8.67

INTERCEPT = -130.64511

MULTIPLE R = 0.4802

MULTIPLE R-SQUARED = 0.2306

ADJUSTED R-SQUARED = 0.2217

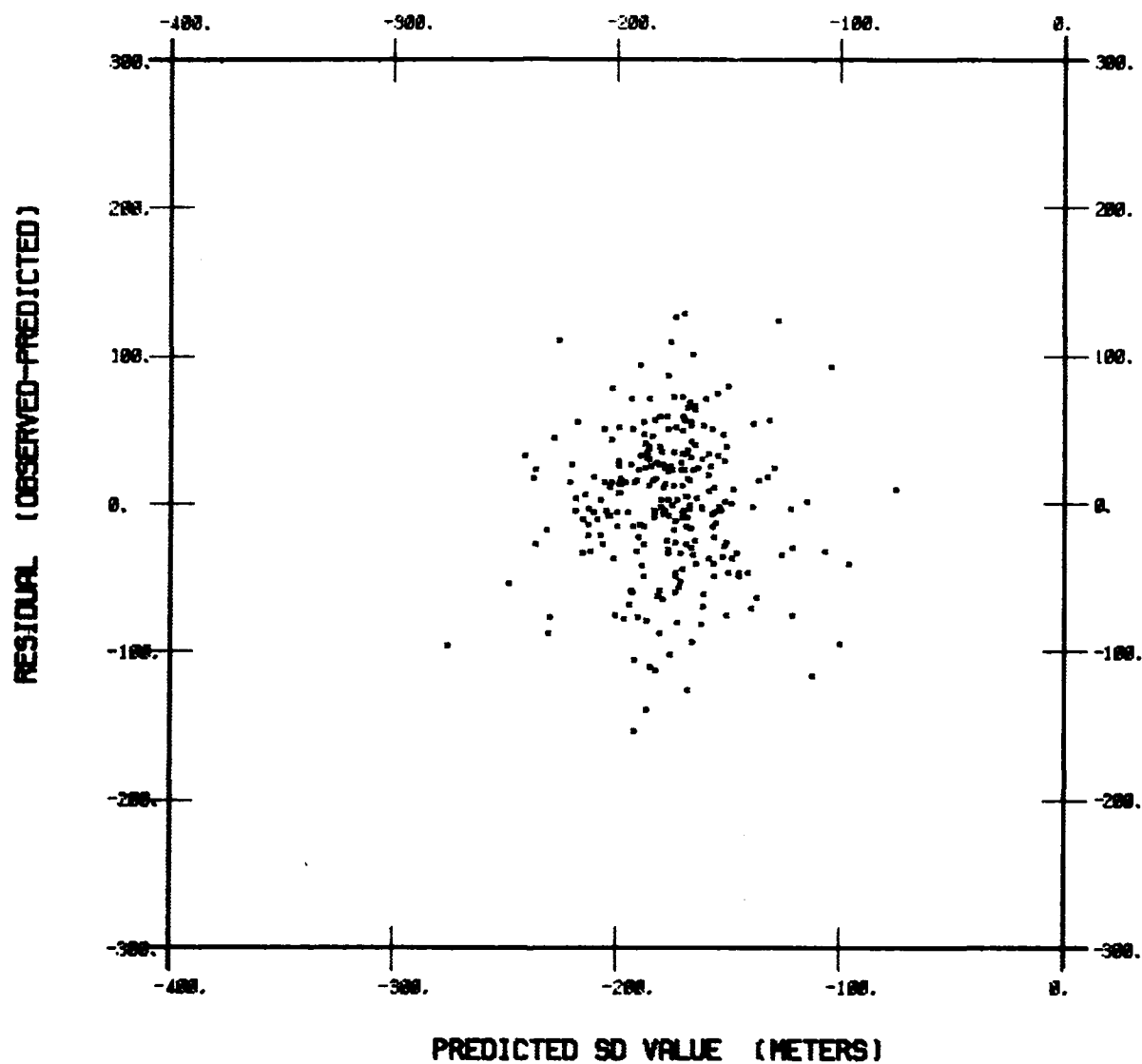


Figure 12. Scatter diagram of the predicted SD value versus the residual for the 1000/300 mb dependent data set (no satellite parameters).

Chapter 5

Verification of Technique

5.1 300 mb Independent Data Set

The basic statistical properties of the variables included in the 123 cases comprising the 300 mb independent data set are shown in Table 10 for comparison with the statistics computed for the 300 mb dependent data set in Table 4.

The 300 mb SD regression equation, including the satellite derived parameters, was used to compute estimates of the magnitudes of the SD extrema of the independent data set. The RMS error of the observed versus predicted SD values for the independent data set was 33.27 meters. A plot of the residuals for the independent data set is given in Figure 13. The residuals for the independent data set appear to have no trends. Therefore, the 300 mb regression model appears to be adequate and stable with no apparent systematic error.

5.2 1000/300 mb Independent Data Set

The basic statistical properties of the variables included in the 115 cases comprising the 1000/300 mb independent data set are shown in Table 11 for comparison with the statistics computed for the 1000/300 mb dependent data set in Table 7.

Table 10.

300 MB : INDEPENDENT DATA SET

VARIABLE	MEAN	STANDARD DEVIATION	SKEWNESS	KURTOSIS
FLAT	.85865	.14973	-.18516	-.47763
FLON	.70092	.36805	.21312	-.79260
SLAT	.87734	.15327	-.09850	-.46271
SLON	.61980	.36222	.19806	-.58390
AMP	3.50483	1.39591	.74888	-.24675
RL	2.88451	1.03516	.77824	-.07641
IST	2.34146	.47420	.66864	-1.55293
SD	-220.39840	55.34015	-.00370	.27860
SRU	18.21138	7.44219	.60404	.30371
SRV	-.65054	6.13370	-.41914	.24612
SVL	3.55631	3.91525	-.70241	-.21135
SLH	-75.00942	91.21101	-.31323	1.30044
SLU	5.52846	6.19116	.01502	.35402
SLV	-.53659	5.78095	-.35753	.39805
SLL	24.97237	20.31718	.23392	1.10163
SVH	71.13820	179.50100	-.73296	-.06124
SVU	12.89431	3.37811	.19871	-.38882
SVV	.21138	.65335	1.32765	4.19123
RLS	2.17079	.76410	.76071	.32208
RL5	1.67234	.29627	.44464	-.47865
RLMA	11.39112	0.56090	1.33408	1.10512
AMDR	1.21830	.23790	.77885	1.54160
RLDA	.85162	.16507	.63477	.65415
RLDC	4.65501	1.64013	.62742	.15502
RLS2	1.66092	.63780	.66818	.42900

123 TOTAL OBSERVATIONS

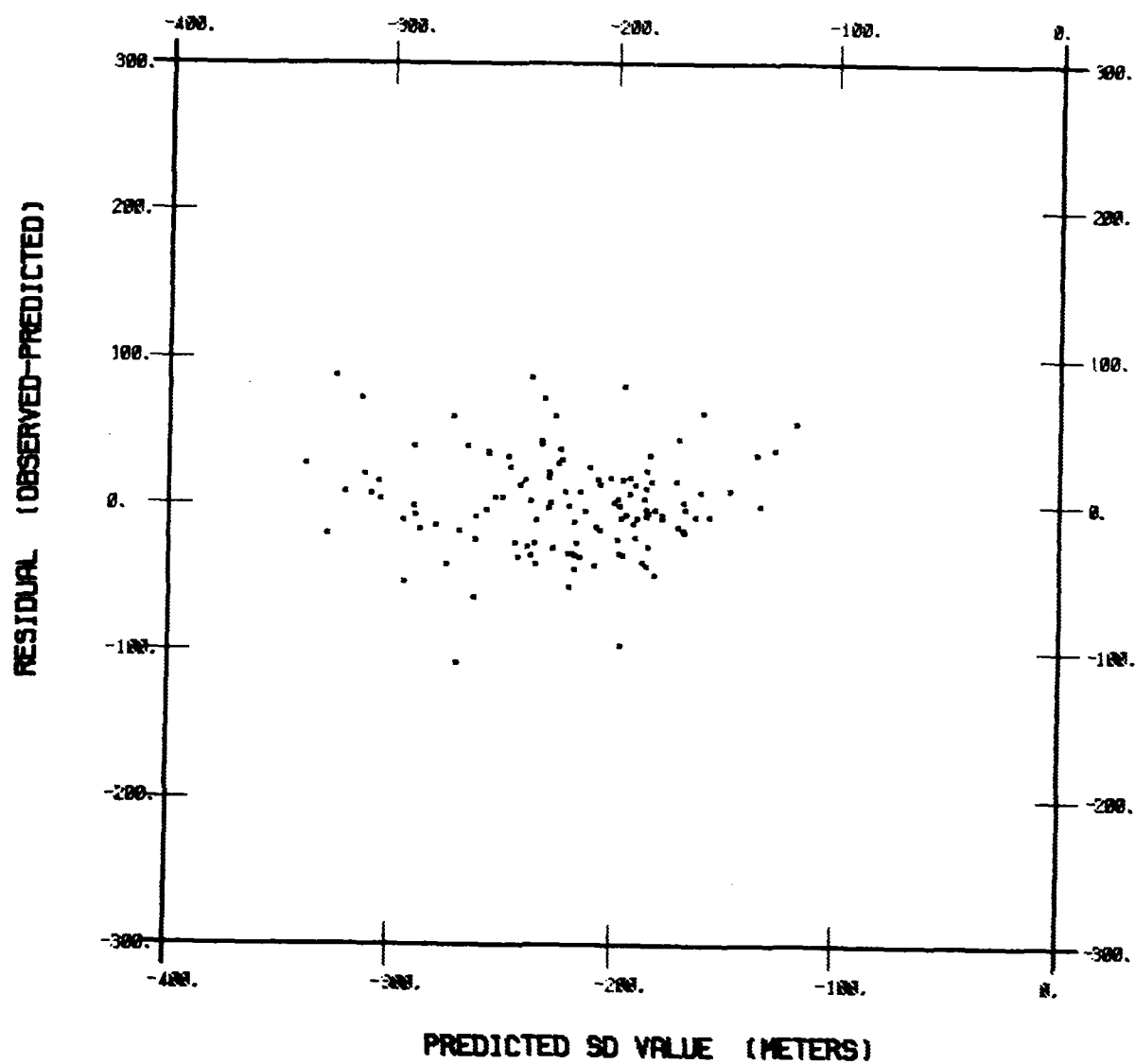


Figure 13. Scatter diagram of the predicted SD value versus the residual for the 300 mb independent data set.

Table 11.

1000/300 MB : INDEPENDENT DATA SET

VARIABLE	MEAN	STANDARD DEVIATION	SKEWNESS	KURTOSIS
FLAT	.79690	.15323	-.20789	.39014
FLON	.71623	.35677	.23777	-.97346
SLAT	.83593	.16644	-.23297	-.07636
SLON	.59932	.34206	.18889	-.99180
AMP	3.32952	1.31369	.95556	.85699
RL	2.80170	.92536	.48727	-.61074
IST	2.36522	.48149	.55985	-1.68658
SD	-163.73910	51.28595	-.04125	-.51925
SRU	16.10434	6.25736	.55837	.12241
SRV	-.26957	6.11103	-.44373	.40937
SVL	2.44304	3.93296	-.52790	.18706
SLH	-34.73912	63.53854	-.20703	.20020
SLU	3.18261	4.91419	.36437	.03167
SLV	-.24348	5.51140	-.38617	.26461
SLL	16.94540	15.26734	-.09495	-.05878
SVH	103.30430	157.83590	-.44509	-.36990
SVU	13.20000	3.65037	.16673	-.53047
SVV	.33913	.74468	1.00293	1.83109
RLS	2.04516	.72214	.34224	-.74936
RLS	1.65122	.27413	.21961	-.85480
RLMA	10.33154	7.33653	1.51171	2.66721
AMDR	1.19500	.28186	1.28466	2.42610
RLDA	.87831	.18548	.17222	-.04934
RLDC	4.34616	1.49327	.31197	-.83532
RLS2	1.52489	.62007	.20735	-.69810

115 TOTAL OBSERVATIONS

The 1000/300 mb SD regression equation, including the satellite derived parameters, was used to compute estimates of the magnitudes of the SD extrema of the independent data set. The RMS error of the observed versus predicted was 32.7 meters. A plot of the residuals for the independent data set is given in Figure 14. The residuals for the independent data set appear to have no trends. Therefore, the 1000/300 mb regression model appears to be adequate and stable with no apparent systematic error.

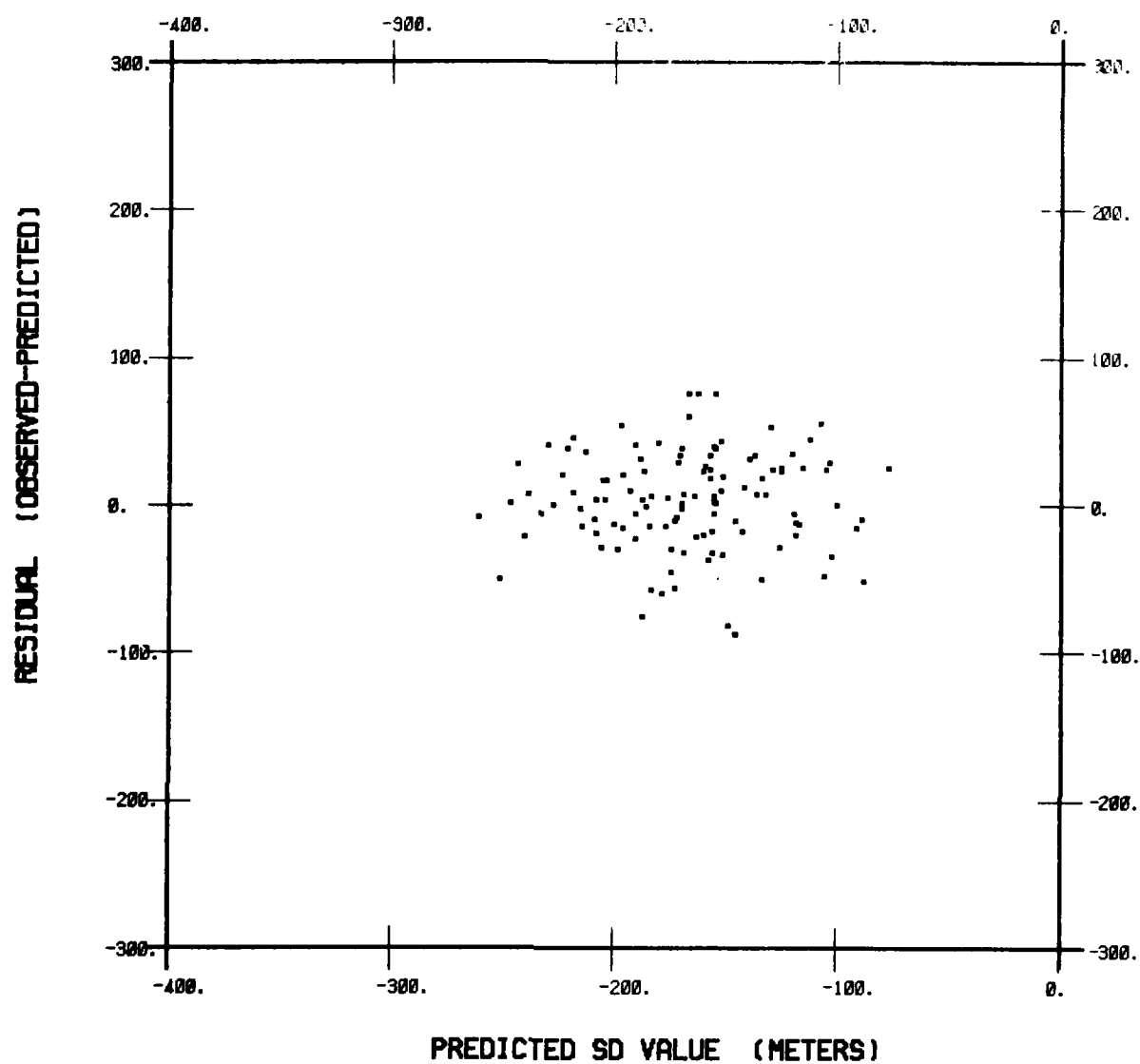


Figure 14. Scatter diagram of the predicted SD value versus the residual for the 1000/300 mb independent data set.

Chapter 6

Conclusions and Recommendations

6.1 Conclusions

The primary objective of the present study was to formulate a quasi-objective technique to derive the magnitudes of the negative extrema of the 300 mb and 1000/300 mb height and thickness short wavelength component fields based upon satellite observed spiral cloud pattern geometry and various long wavelength field parameters. It was shown that quantitative use of satellite observed spiral cloud patterns and parameters derived from the long wavelength fields can be made in modifying the 300 mb and 1000/300 mb height and thickness fields. Proper interpretation of the satellite imagery permits the identification and location of the short wavelength systems in the 300 mb and 1000/300 mb fields. The regression equations, including the satellite parameters as predictors, permit quantitative estimates of the magnitudes of the negative extrema in the short wavelength 300 mb and 1000/300 mb fields.

The multiple regression correlation coefficient for the 300 mb data shows little appreciable difference compared to Nagle and Hayden's correlation coefficient for the 500 mb field (0.31 versus 0.80 respectively). The root mean squared (RMS) error of 30.9 meters for the 300 mb

independent data set is appreciably lower than the RMS error of 41 meters for Nagle and Hayden's 500 mb independent data set. The 300 mb height analysis using surface, radiosonde height and satellite vertical temperature profiles has a RMS error of 10.6 meters when computed for the relatively dense data network of Northern Europe (Murphy and Williamson, 1976). This can be considered as the inherent error in the current "perfect" analysis. The RMS error value of the predicted (the "first guess") 300 mb heights as given by Rutherford (1976) is 32.7 meters computed for the entire northern hemisphere. This implies that the RMS height error over data sparse areas can exceed 40 meters. Therefore, the technique developed in the present study can significantly improve the accuracy of the 300 mb geopotential height field in data sparse regions.

Upon examining the 1000/300 mb thickness field RMS height error of 32.7 meters in light of the above discussion, it appears that the present technique can also significantly aid the analysis in data sparse areas. Equally important is that the 1000/300 mb thicknesses estimated by this technique can insure vertical consistency of the mass field which is an essential requirement for initializing a multi-level primitive equation model.

The regression equations developed excluding the satellite parameters can be used when specification of the cloud parameters is ambiguous. The estimates of the SD

values computed with these regression models are conservative estimates with larger RMS errors than associated with the regression models including the satellite parameters. These equations could be used for systems in the formative stage of development when the interpretation of the satellite image is difficult, and requires considerable subjectivity.

Therefore, provided the satellite images are properly interpreted and that the long wavelength component fields provided by the 12-hr numerical forecasts can be accepted as a reasonable base, the technique developed in the present study can significantly improve the accuracy of the 300 mb and 1000/300 mb geopotential height and thickness fields in data sparse regions. Appendix C provides the details for adapting these techniques for operational usage.

6.2 Recommendations for Future Study

Verification of the zero line positioning and testing of the techniques to define the spatial characteristics of the 300 mb and 1000/300 mb SD fields should be further explored. This will require satellite imagery (preferably from a geostationary satellite, in order to avoid problems associated with mosaics) valid at analysis times. The spatial errors between the satellite image and the field analysis would then be at a minimum.

The impact of this technique on a regional or global

numerical model, and the ability of the objective analysis and initialization schemes to retain the adjustments to the fields should be pursued. However, if the impact is neutral or negative, an explanation may be that the additional satellite information provided by this technique are not being exploited fully by the existing system. This is quite probable if the existing system has been designed primarily for assimilating synoptic rawinsonde data. Finally, assessments of the impact should be qualitative as well as statistical, should discriminate according to geographical area and space time scales, and should give emphasis to synoptically active test situations.

APPENDIX A

1. Properties of Scale Separation

The smoothing filter is defined by

$$\phi \equiv \phi_0 + \delta^2 \int_0^\alpha \nabla^2 \phi \, d\alpha \quad (\text{A1})$$

where ϕ is the smoothed field, ϕ_0 is the original field, δ is a constant, ∇^2 the two-dimensional Laplacian operator, and α is the degree of smoothing (Holl, 1963). Equation (A1) may be expressed in a more general operator notation as

$$\phi[\alpha] = \phi[0] - \phi[0, \alpha] \quad (\text{A2})$$

where $\phi[\alpha]$ is the field ϕ smoothed to degree of smoothing α , and $\phi[0, \alpha]$ is the residual field resulting from the smoothing operating on the ϕ field from its initial state $\alpha = 0$ to the final state $\alpha = \alpha$.

The properties of the smoother can be examined by assuming the ϕ field can be represented by a one-dimensional Fourier component with wave-number k and

whose amplitude A_k will be a function of the degree of smoothing. Equation (A1) can be written in differential form as

$$\frac{\partial \phi}{\partial \alpha} = \delta^2 \nabla^2 \phi \quad . \quad (A3)$$

The one-dimensional Fourier component is expressed by

$$\phi[0] = A_k[0] e^{ik\alpha} \quad (A4)$$

where $i = \sqrt{-1}$. Substituting (A4) into (A3) and solving yields

$$\phi[\alpha] = \phi[0] e^{-k^2 \delta^2 \alpha} \quad (A5)$$

$$A_k[\alpha] = A_k[0] e^{-k^2 \delta^2 \alpha} \quad (A6)$$

The amplitude reduction factor which is a function of the degree of smoothing and wave-number is given by

$$R = \frac{A_k[\alpha]}{A_k[0]} = e^{-k^2 \delta^2 \alpha} \quad . \quad (A7)$$

The larger the degree of smoothing (large α) the more the amplitude will be reduced. It is readily seen that for a given degree of smoothing the shorter waves' (large k) amplitudes are greatly reduced.

2. Analysis of the Numerical Analogue

Computationally Equation (A1) is integrated by repeated applications of the Laplacian operator with varying increments in $\alpha(\alpha_1, \alpha_2, \dots, \alpha_n)$. Using Equation (A5) one can show that the resultant smoothing is cumulative in α , since

$$\begin{aligned}\phi[\alpha_1][\alpha_2] &= \phi[0][\alpha_2] e^{-k^2 \delta^2 \alpha_1} \\ &= \phi[0] e^{-k^2 \delta^2 (\alpha_1 + \alpha_2)} \\ &= \phi[\alpha_1 + \alpha_2] .\end{aligned}\tag{A8}$$

The explicit finite difference analogue of Equation (A8) is:

$$\begin{aligned}\phi[\alpha_1] &= \phi[0] + \tau^2 \phi[0] \alpha_1 \\ \phi[\alpha_1 + \alpha_2] &= \phi[\alpha_1] + \tau^2 \phi[\alpha_1] \alpha_2 ,\end{aligned}\tag{A9}$$

or in general for the nth degree of smoothing:

$$\phi\left[\sum_{i=1}^n \alpha_i\right] = \phi\left[\sum_{i=1}^{n-1} \alpha_i\right] + \tau^2 \phi\left[\sum_{i=1}^{n-1} \alpha_i\right] \alpha_n ,\tag{A10}$$

where ∇^2 is the five-point finite difference approximation of the Laplacian operator on a lattice with gridlength δ . For reasons of numerical stability the α_i 's increase with successive steps.

The smoothing of degree α is complete when the sum of the α_i 's reaches the predetermined value. $\phi[\alpha]$ is the long-wave component field and $\phi[0] - \phi[\alpha]$ is the short-wave component field.

Equation (A7) can be used to construct a filter (smoother) response curve where the wave-number is replaced by wavelengths in grid increments, i.e.

$$k = 2\pi(n\delta)^{-1}. \quad (\text{A11})$$

The amplitude reduction factor becomes

$$R = e^{-4\pi^2 \alpha / n^2} \quad (\text{A12})$$

Using Equation (A12) a family of curves corresponding to different α for the reduction factor as a function of n can be constructed. However, a single more general curve can be derived by introducing a new variable x which is a function of both α and n :

$$rx^2 = 4\pi^2 \alpha / n^2 \quad (\text{A13})$$

where r is an arbitrary positive constant used to scale x . Equation (A12) can be rewritten as

$$R = e^{-rx^2} . \quad (A14)$$

For plotting purposes the constant r was chosen by requiring that $R = 0.5$ when $x = 1.0$, which leads to the numerical value for r of 0.693147. The filter curve for this scheme is shown by the solid line in Figure 15.

An ideal filter would be a vertical line at $x = 1.0$. The filtering technique described above is known as first-order smoothing and is not as sharp as the ideal filter. The resulting long-wavelength field contains some short-wavelength components and vice versa. The application of higher order filters can compensate this undesirable feature at the expense of computation time.

The concept of higher order smoothing is demonstrated with the following example. Suppose that after applying first-order smoothing, the short-wavelength field contains 95 percent of the amplitude of a given short wave and erroneously contains 15 percent of the amplitude of a given long wave, due to the imperfect first order filter.

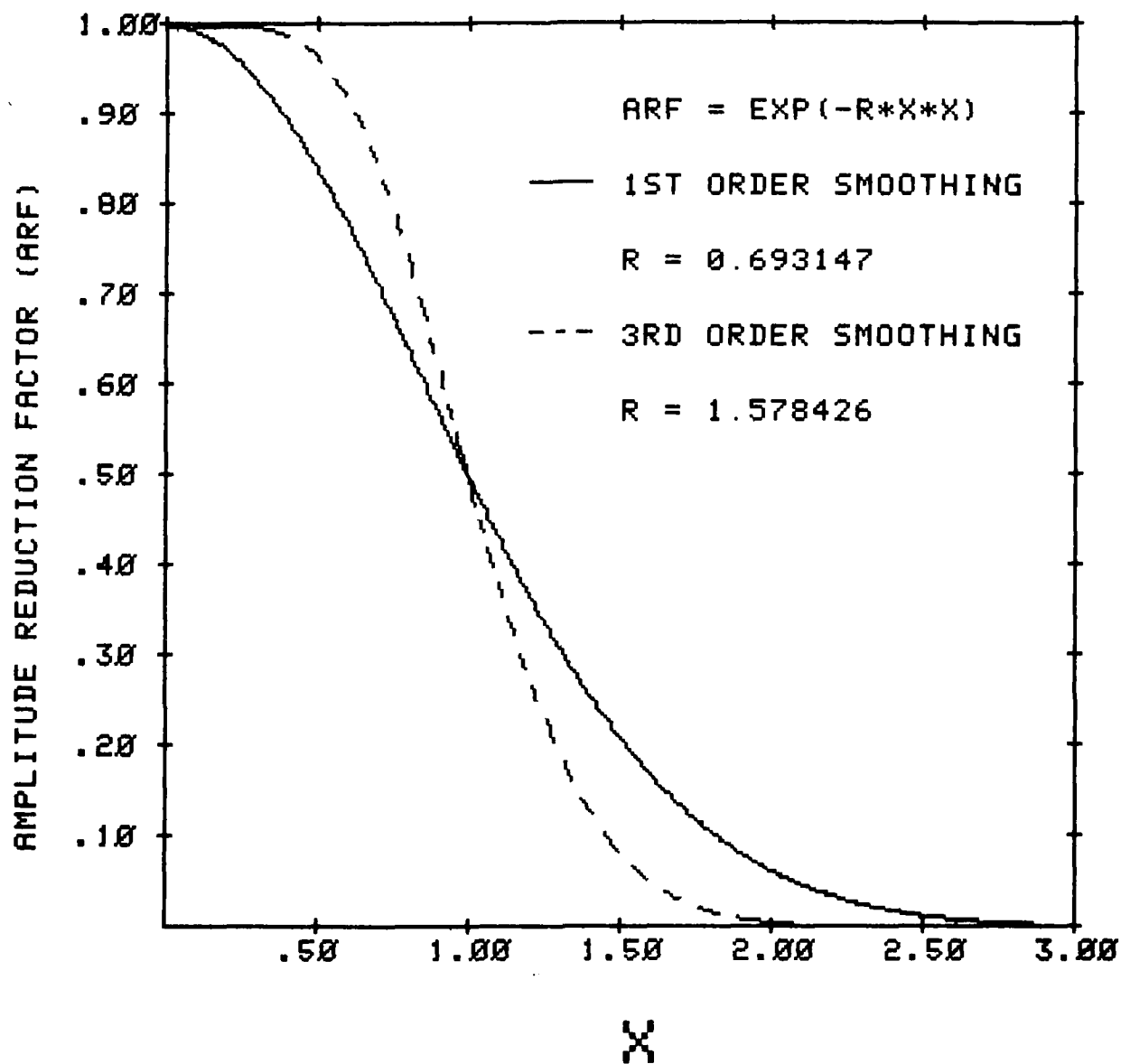


Figure 15. Normalized filter curves for 1st and 3rd order smoothing.

If the filtering process is now applied to the short-wavelength field, to yield large and small scale components, the amplitude of the long wave will be reduced in the second short-wavelength component field to 0.15×0.15 or 2.25 percent of its original amplitude. The short wave amplitude will be reduced in the second short-wavelength component field to 0.95×0.95 or 90.25 percent of its original amplitude. This second-order smoothing is much sharper than the first order because the longer wavelengths are filtered more rapidly than the shorter wavelengths.

3. Second Order Smoothing

Equation (A2) for first-order smoothing can be rewritten as:

$$\phi[0,x] = \phi[0] - \phi[x] \quad . \quad (A15)$$

Second-order smoothing involves smoothing the residual field a second time:

$$\begin{aligned} \phi[0,x][0,x] &= (\phi[0] - \phi[x])[0,x] \\ &= \phi[0][0] - \phi[0][x] - \phi[x][0] + \phi[x][x]. \end{aligned} \quad (A16)$$

From Equation (A8)

$$\phi[0,\alpha][0,\alpha] = \phi[0] - 2\phi[\alpha] + \phi[2\alpha]. \quad (\text{A17})$$

Adopting the convention

$$\phi[\alpha][\alpha] = \phi[2\alpha] = \phi[\alpha]^2. \quad (\text{A18})$$

Equation (A17) can be written as:

$$\phi[0,\alpha]^2 = \phi(1 - [\alpha])^2 \quad (\text{A19})$$

or in general

$$\phi[0,\alpha]^n = \phi(1 - [\alpha])^n. \quad (\text{A20})$$

The resulting long-wavelength component field after n th degree of smoothing is:

$$\begin{aligned} \phi_{\text{LW}} &= \phi[0] - \phi[0,\alpha]^n \\ &= \phi\{1 - (1 - [\alpha])^n\}. \end{aligned} \quad (\text{A21})$$

The smoothing process used for this study was third-order smoothing. The long-wavelength field is given by

$$\phi_{\text{LW}} = 3\phi[\alpha] - 3\phi[2\alpha] + \phi[3\alpha]. \quad (\text{A22})$$

Equation (A22) shows that in practice the field is smoothed to 3λ rather than by repeated smoothing, which computationally is more efficient.

The amplitude reduction factor for third-order smoothing is

$$R = 3e^{-rx^2} - 3e^{-2rx^2} + e^{-3rx^2} . \quad (A23)$$

By requiring that $R = 0.5$ when $x = 1.0$ the numerical value of the constant r is 1.5784264 . Figure 15 shows that third order smoothing is indeed sharper than first order. Using Equation (A23) and the definition of r , the corresponding degree of smoothing is $\lambda = 8.52$.

Equation (A1) defines the procedure for explicit smoothing. However, implicit smoothing is found to be more efficient and is used in practice. One smoothing cycle is represented by

$$u[n+d\lambda] = u[n] + \frac{d\lambda}{2} \nabla^2 u[n] + \frac{d\lambda^2}{2} \nabla^4 u[n] \quad A24$$

Equation (A24) is solved by standard overrelaxation. The optimum relaxation factor (Holl, 1967) ω is given by:

$$\omega = 1 + \left[\frac{\bar{q}^2}{1 + (1 - \bar{q}^2)^{1/2}} \right]^2 \quad (\text{A25})$$

where

$$\bar{q} = 2\delta\alpha / (2\delta\alpha + 1) \quad . \quad (\text{A26})$$

The number of iterations required for adequate accuracy is

$$N \geq \frac{\ln 0.02}{\ln (\omega - 1)} \quad . \quad (\text{A27})$$

The $\delta\alpha$ for each smoothing cycle is defined such that after 15 cycles the fields will be smoothed to α , 2α , and 3α . A normalized table for $\delta\alpha_*$ is given in Table 12. The actual $\delta\alpha$ used for each cycle is found by multiplication of the normalized value and the desired degree of smoothing.

TABLE 12

12. Normalized smoothing increments (after Holl, 1967)

Cycle No.	δa_*	Σa_*
1	0.006	0.006
2	0.009	0.015
3	0.014	0.029
4	0.020	0.049
5	0.030	0.079
6	0.045	0.124
7	0.068	0.192
8	0.102	0.294
9	0.154	0.448
10	0.230	0.678
11	0.322	1.000
12	0.500	1.500
13	0.500	2.000
14	0.500	2.500
15	0.500	3.000

APPENDIX B

The linear regression of y on the variable x can be extended to the multiple regression

$$y = \beta_1 X_1 + \beta_2 X_2 + \dots + \beta_n X_n = \sum_{j=1}^n \beta_j X_j, \quad (B1)$$

where X_1, X_2, \dots, X_n are the n different variables and $\beta_1, \beta_2, \dots, \beta_n$ are the model parameters of the regression line. The special case in which X_1 is identically one, would mean that β_1 had now assumed the role of the regression constant or y -intercept. Suppose that M experimental observations are made and that X_{ij} is the value of the variable X_j at the i th observation. Letting Y_i be the i th observed value of y , the formulation of the multiple regression procedure requires one to minimize the sum of squares

$$S = \sum_{i=1}^M (Y_i - \sum_{j=1}^n \beta_j X_{ij})^2. \quad (B2)$$

Setting $\partial S / \partial \beta_k = 0$ for $k = 1, 2, \dots, n$, and replacing the β_j , with their least-squares estimates b_j , we have

$$\sum_{i=1}^M X_{ik} (Y_i - \sum_{j=1}^n b_j X_{ij}) = 0$$

That is,

$$\sum_{j=1}^n b_j \sum_{i=1}^M x_{ik} y_{ij} = \sum_{i=1}^M x_{ik} y_i, \quad (B1)$$

$$k = 1, 2, \dots, n.$$

Now define \tilde{X} as the $M \times n$ matrix containing x_{ij} in its i th row and j th column:

$$\tilde{X} = (x_{ij}) = \begin{bmatrix} x_{11} & \cdot & \cdot & \cdot & x_{1n} \\ \cdot & \cdot & & & \\ \cdot & & \cdot & & \\ \cdot & & & \cdot & \\ \cdot & & & & \cdot \\ x_{M,1} & & & & x_{M,n} \end{bmatrix} \quad (B4)$$

The following column vectors are also defined:

$$y = [y_1 \ y_2 \ \dots \ y_n]^t \quad (B5)$$

$$b = [b_1 \ b_2 \ \dots \ b_n]^t \quad (B6)$$

Where the superscript t denotes the transpose of the vector. The system of normal equations (B3) can be expressed as:

$$\tilde{X}^t \tilde{X} b = \tilde{X}^t y \quad (B7)$$

which has the solution

$$\tilde{b} = (\tilde{X}^t \tilde{X})^{-1} \tilde{X}^t \tilde{y} .$$

The $M \times n$ symmetrical variance-covariance matrix V is defined by

$$\tilde{V} = (v_{ij}) = (\tilde{X}^t \tilde{X})^{-1} \sigma^2 , \quad (B9)$$

where σ^2 is estimated from

$$s^2 = \frac{\tilde{y}^t \tilde{y} - \tilde{b}^t \tilde{X}^t \tilde{y}}{M - n} . \quad (B10)$$

The diagonal and off-diagonal elements of V give, respectively, the variances and covariances of the b_j ; that is,

$$\text{var}(b_j) = v_{jj} , \text{ and } \text{cov}(b_i, b_j) = v_{ij} .$$

The system of normal equations (B3) can be solved by any number of conventional methods such as Gaussian elimination or matrix inversion.

In the present study, the Biomedical Computer Programs P-Series (BMDP-79) library developed at the Health Sciences Computing Facility at the University of California at

Los Angeles was used (Dixon and Brown, 1979). The stepwise multiple regression program P2R was employed for the regression analysis..

P2R computes estimates of the parameters of a multiple linear regression equation in a stepwise manner. The variables are entered (forward stepping) or removed (backward stepping) from the equation one at a time according to any of four possible criteria. Univariate statistics computed for each variable are: mean, standard deviation, coefficient of variation, skewness, kurtosis, maximum, and minimum values. Results are printed at each step along with the multiple correlation coefficient R (i.e. the correlation of the dependent variable \hat{y} with the predicted value y) as well as the multiple R^2 , the adjusted RA^2 given by

$$RA^2 = R^2 - n(1 - R^2)/(M - n) \quad (B11)$$

(Thiel, 1971), and the standard error estimate given by:

$$e_s = \left[\sum_{j=1}^M \frac{(y_j - \hat{y}_j)^2}{M - n} \right]^{1/2} \quad (B12)$$

The analysis of variance table containing the regression sums of squares, residual sums of squares and the F ratio,

inclusion in the equation in a manner that maximizes the F ratio, the level of significance of the F ratio cannot be obtained from an F distribution.

Any one of four methods can be used for entering or removing variables from the equation at each step. The methods are:

F The variable with the smallest F-to-Remove, given by:

$$\frac{SS(\text{residuals if variable is removed}) - SS(\text{residuals})}{SS(\text{residuals}) / (M - n)}$$

Where SS is the sum of squares, is removed if its F-to-remove is lower than the specified F-to-remove limit. If no variable meets this criterion, the variable with the largest F-to-enter defined by

$$\frac{SS(\text{residuals}) - SS(\text{residuals after next step})}{SS(\text{residuals after next step}) / (M - n - 1)},$$

is entered if the F-to-enter value exceeds the specified F-to-enter limit.

SWAP Same as method F above, except when no variable meets the F-to-remove criterion, a variable in the equation is exchanged with a variable not yet in the equation if the exchange increases

the multiple regression correlation coefficient R . If no variable can be exchanged, a variable is entered as in F.

R The variable with the smallest F-to-remove is removed if its removal results in a larger multiple R than was previously obtained for the same number of variables. If no variable meets this criterion, a variable is entered as in F.

RSWAP Same as method R, except when no variable meets this criterion, a variable in the equation is exchanged with a variable not yet in the equation if the exchange increases the multiple correlation coefficient R . If no variable can be exchanged, a variable is entered as in F.

The method F requires the fewest computations.

Since all four methods begin with no variables in the equation, they appear to describe a forward stepping algorithm. The F-to-enter and F-to-remove limits can each be assigned two values. The first pair is used until all variables that meet the criteria have been entered; the second pair of limits is then used to remove the variable (backward stepping). By assigning very low values to the

first pair of limits, all (or nearly all) variables can be entered into the equation. By assigning high values to the second pair, the variables in the equation can be removed.

A possible danger involved in this method is that, as the number of predictors n increases, the further increase in the model's explained variance may be due not to physical relationships but rather due to chance relationships in the data sample that may not exist in other samples. Panofsky and Brier (1968) refer to this as "overfitting". To prevent this the data were randomly divided into two groups: two-thirds of the observations were used as the dependent data set, while the remaining one-third became the independent set. The various regression models were applied to the independent set, with the model yielding the largest reduction in variance selected as the best regression equation. An example of the P2R program control information used for this study is shown in Figure 16.

PROGRAM CONTROL INFORMATION

```

/PROBLEM      TITLE IS 300 MB SD SINAP REGRESSION .
/INPUT        VARIABLES = 19.
              FORMAT = (6X,6E14.6,2X,I1,/,12E10.3) .
              UNIT = 20.
/VARIABLE     NAMES ARE FLAT,FLON,SLAT,SLON,AMP,RL,IST,SD,SRU,
              SRV,SVL,SLH,SLU,SLV,SLL,SVH,SVU,SVV,SVL,RLS,RL5,
              RLMA,AMDR,RLDA,RLDC,RLS2.
              ADD = 7.
/TRAN        RLS = RL*SIN(SLAT).
              RL5 = SORT(PL).
              RLMA = RL*AMP.
              AMDR = AMP/RL.
              RLDA = RL/AMP.
              RLDC = RL/COS(SLAT).
              RLS2 = RL*SIN(SLAT)*SIN(SLAT).
/REGRESS     DEPEND = SD.
              INDEP = SLAT,SLON,AMP,RL,SRU,SRV,SVL,SLH,SLU,SLV,
              SLL,SVH,SVU,SVV,SVL,RLS,RL5,FLMA,AMDR,RLDA,RLDC,
              RLS2.
              TITLE = FORWARD STEPPING MULTIPLE REGRESSION .
              METHOD = F.
              ENTER = 4.0.
              REMOVE = 3.9.
              TOL = 0.05.
/PRINT       DATA.
              CORR.
/END.

```

BMDP UNIT NO. 20 SPECIFIED IN THE INPUT PARAGRAPH WILL REFER TO LOCAL FILE NAME TAPE20 FOR THIS PROBLEM.

Figure 16. P2R program control language.

APPENDIX C

The operational application of the technique developed in the present study and described herein, is designed to utilize the Naval Environmental Prediction Research Facility's Satellite-Data Processing and Display System's (SPADS) unique capabilities of allowing interactive digital image processing (Schramm, Zeleny, Nagle, and Weinstein, 1982). Graphic overlays of the meteorological fields superimposed upon the satellite image make this system ideal for the application of the present technique.

Since parameters derived from the long wavelength field are required for the regression models for estimating the magnitudes of the negative extrema of the SD field, it must be assumed that the long wavelength field is accurately specified. In a realtime application the current long wavelength analysis is not available, but rather the 12-hr numerical forecast of the fields are to be used. The assumption being that the 12-hr forecast (the "first guess") contains sufficient information for accurate specification of the long wavelength fields. Nagle and Hayden tested this assumption by comparing the differences between the 12-hr first guess field and subsequent analysis for 500 mb height fields. They also compared the differences of the Laplacians of the fields and found in both cases the errors were acceptably low for use in the current context.

The primary satellite data used will be digital satellite imagery obtained from the geostationary satellites of the GOES series. The 12-hr numerical 300 mb and 1000/300 mb forecast fields are computer processed to produce the SV, SR, SL and SD fields. Selection of the GOES image sector within the hour preceeding the analysis time (i.e. 1200 or 000 GMT) is then made and the image displayed. The analyst then interprets the spiral cloud system by defining the parameters required by the regression equation. Once the analyst is satisfied with the defined spiral parameters, the value of the SD extrema is then computed.

The zero line defining the region of influence of the computed SD feature is then defined along the amplitude and wavelength axes designated by graphical means on the color monitor. The zero line intersects these lines at the inner edge of the major frontal cloud band. This defines the major and minor axes of an ellipse that can be used to approximate the SD feature. Another possibility, would be to simply define the position of the zero line with the graph pen and pad. The SD feature could then be defined by the following relationship

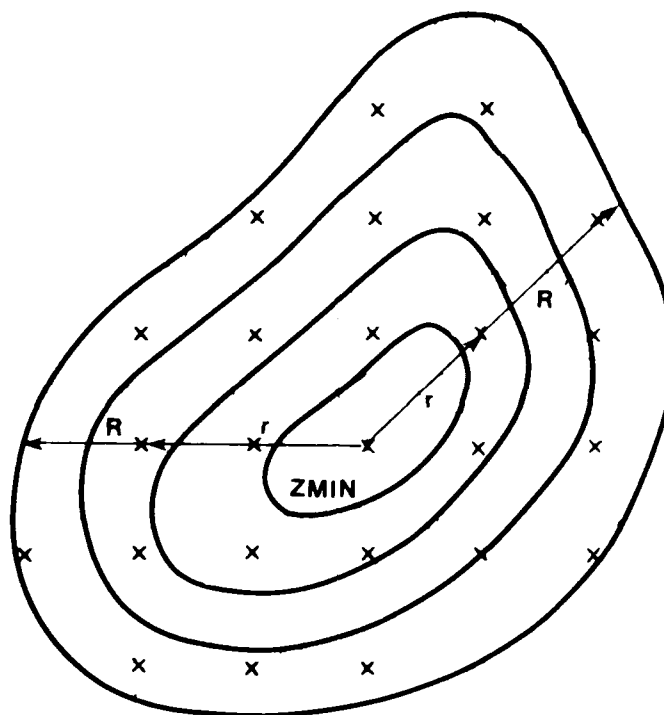
$$Z = Z_{\min} \cos (Tr/2R),$$

where Z is the value at the grid point defined by r, where r is the distance from the center to the grid point, R is the distance from the center to the zero line passing through the grid point and Z_{\min} is the SD value computed at the

regression equation. Figure 17 is a schematic representation of the above.

Once the region of influence is defined, the SD values at the grid points within the region of influence when added to the SR field compose an array of bogus height or thickness values to be blended with the rawinsonde and aircraft data used for the analysis. This procedure can also be used for the 6-hr update cycles when an explosive case of cyclogenesis is apparent in the satellite imagery but not reflected in the twice daily analysis times. A schematic of this SINAP¹ process is shown in figure 18.

1 SINAP: Satellite Input to Numerical Analysis and Prediction



$$Z = ZMIN \cdot \cos[\pi r / 2R]$$

Figure 17. Schematic representation of a SD feature approximating function.

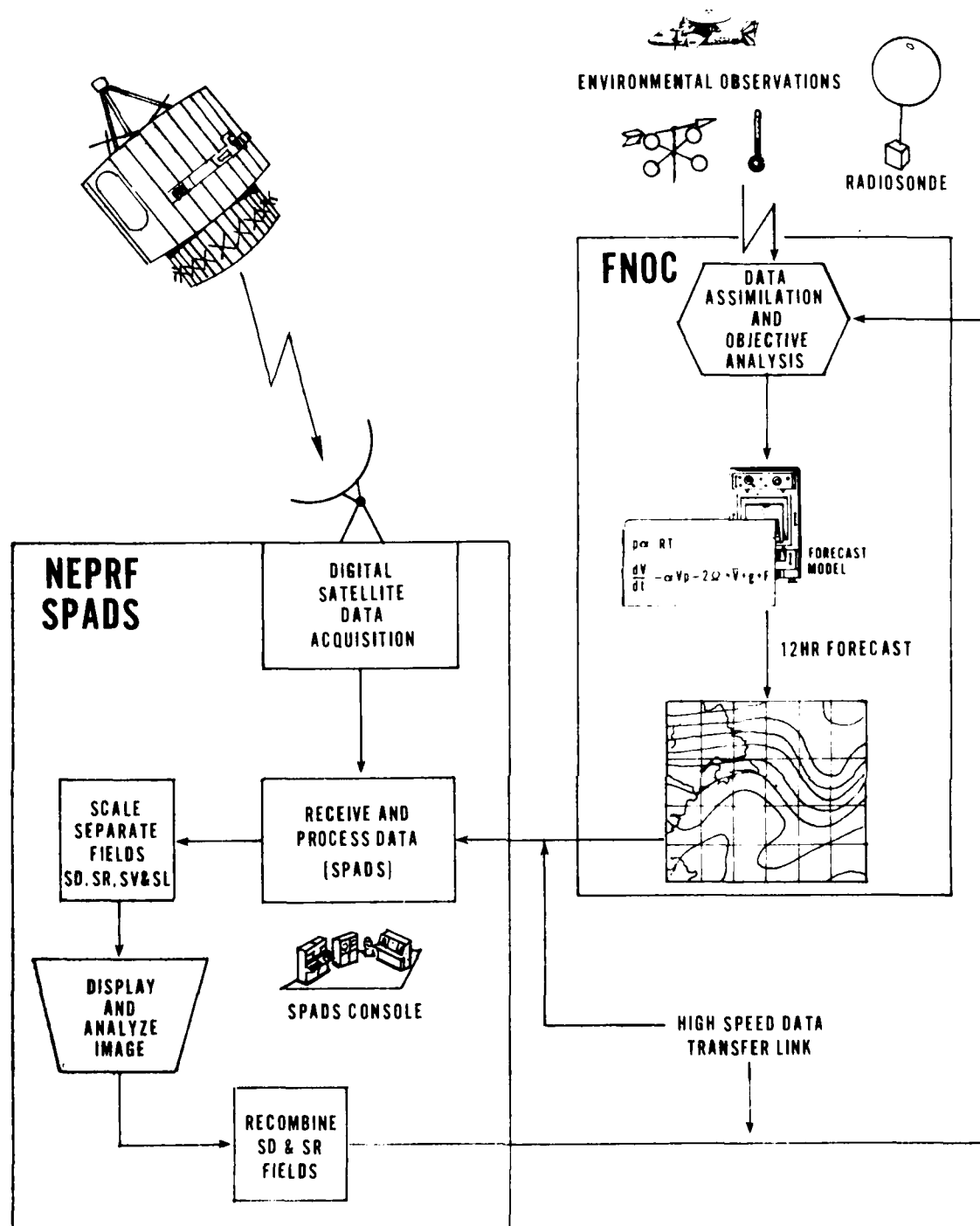


Figure 18. Schematic flow diagram for the operational usage of the SINAP technique.

References

- Afifi, A.A. and Azen, S.P., 1979: Statistical Analysis: A computer oriented approach. Academic Press, New York. 442 pp.
- Barr, S., Lawrence, M. and Sanders, F., 1966: TIRCC Vortices and Large Scale Vertical Motion. Mon. Wea. Rev., 94, 675-696.
- Bizzarri, B., 1982: Satellite Data for Numerical Weather Prediction. Revista Meteorologia Aeronautica, 42, 369-382.
- Bradley, J.H.S., Hayden, C.M. and Wiin-Nielsen, A.C., 1966: An Attempt to Use Satellite Photography in Numerical Prediction. Final Report, Contract CWB 11145, University of Michigan.
- Broderick, H.J., 1969: Some Aspects of the Vorticity Structure Associated with Extratropical Cloud Systems. ESSA Tech. Mem. NESCTM 15, 8pp.
- Carnahan, B., Luther, H.A. and Wildes, J.O., 1969: Applied Numerical Methods. John Wiley & Sons, Inc. New York. 608pp.
- Dixon, W.J. and Brown, M.B., 1979: Biomedical Computer Programs P-Series, (BMDP-79). University of California Press, Berkeley, 880pp.
- Fjortoft, R., 1952: On a Numerical Method of Integrating the Barotropic Vorticity Equation. Tellus, 4, 179-194.
- Halem, M., Ghil, M., Atlas, R., Susskind, J., and Quirk, W.J., 1977: The GISS Sounding Temperature Impact Test. Final Report Goddard Space Flight Center, NASA 80pp.
- Holl, M.M., 1963: Scale and Pattern Spectra Decompositions. Technical Memorandum No. 3, Contract N00228-62271-47540, Meteorology International Inc., Monterey, CA.
- Holl, M.M., 1967: Inherent-Scale Techniques: A New Version of the Beta Program for an 89x89 Grid. Technical Note No. 1, Contract N00228-67-C-2759, Meteorology International Inc., Monterey, CA.

- Krishnamurti, T.N., 1966: On the Partitioning of the Baroclinic Vertical Motions in a Developing Wave Cyclone. Sci. Rep. No. 1, U.S. Air Force Contract No. AF 19(628)4777, 33 pp. Dept. of Meteorology, Univ. of Cal. at Los Angeles.
- Landsberg, H., 1964: Physical Climatology. Gray Printing Co., Inc. Du Bois, Pennsylvania. 446pp.
- Lowe, P.R., 1983: Personal Communication.
- McClain, E.P., Ruzecki, M.A., and Broderick, H.J., 1965: Experimental use of Satellite Pictures in Numerical Prediction. Mon. Wea. Rev., 93, 445-452.
- Miller, A.J., and Hayden, C.M., 1978: The Impact of Satellite-Derived Temperature Profiles on the Energetics of NMC Analyses and Forecasts During the August 1975 Data Systems Test. Mon. Wea. Rev., 106, 390-398.
- Murphy, A. and Williamson, D., 1976: Weather Forecasting and Weather Forecasts: Models, Systems and Users - Volume 1. Notes from a Colloquium: Summer 1976. 446pp.
- Nagle, R.E. and Hayden, C.M., 1971: The Use of Satellite-Observed Cloud Patterns in Northern-Hemisphere 500 mb Numerical Analysis. NOAA Technical Report NESS 55, 46pp.
- Nagle, R.E., Clark, J.R., and Riegel, C.A., 1966: Objective Assembly of Meteorological Satellite Information. Final Report, Contract N62306-1775, Meteorology International Inc., Monterey, CA.
- Panofsky, H.A. and Brier, G.W., 1968: Some Applications of Statistics to Meteorology. University Park, Pennsylvania State University Press, Pennsylvania, 224pp.
- Rutherford, I.D., 1976: An Operational Three-Dimensional Multivariate Statistical Analysis Scheme. Proceedings, JOC Study Group Conference on Four-Dimensional Data Assimilation. The GARP Program on Numerical Experimentation. Report No. 11, 98-121.
- Schramm, W., Zeleny, P., Nagle, R.E., and Weinstein, A.I., 1982: The Navy SPADS, A Second Generation Environmental Display System. Ninth Conf. Weather Forecasting and Analysis, Seattle, WA.

Seaman, R.S. and Hayden, C.M., 1979: Application of Quantitative Satellite Data to Numerical Analysis and Prediction. Technical Note No. 166, World Meteorological Organization. 87-99.

Thiel, H., 1971: Principles of Economics, New York, Wiley Press, 235pp.

Tracton, S., 1977: The Impact of Satellite Soundings Upon the NMC Analysis and Forecast System. Preprints Third Conference Numerical Weather Prediction, Omaha, Amer. Meteor. Soc., 431-433.

ACKNOWLEDGEMENTS

The author wishes to thank Mr. Roland E. Nagle of the Naval Environmental Prediction Research Facility (NEPRF) for the opportunity to perform the present research, for his many helpful suggestions concerning the analysis procedure and for the time and effort he devoted to it as Principal Investigator and Thesis Committee member.

Special thanks is also extended to Dr. Peter F. Lester and Mr. Sydney M. Serebreny of the San Jose State University Department of Meteorology for being members of the Thesis Committee with the former acting as the Principal Thesis Advisor.

The author also wishes to acknowledge the assistance of several people in obtaining and managing the data utilized: Dr. Eve Schwartz, Mr. Thomas J. Kleespies and Mr. Ronald J. Sznaider of NEPRF, Mr. Michael McDermet of the Naval Post Graduate School, Department of Meteorology, and Ms. Terry Hart of Environmental Data Services.

Thanks is also extended to Ms. Rosie L. Aguon in manuscript word processing, Mr. Stephen Bishop in editorial services and DMI Frank Hermosa in graphics.

This research was conducted under the sponsorship of NEPRF - a Naval Air Systems Command field activity.

DISTRIBUTION

COMMANDER IN CHIEF
U.S. ATLANTIC FLEET
CODE N04E
NORFOLK, VA 23511

COMTHIRDFLT
ATTN: NSAP SCIENCE ADVISOR
CODE N702/01T
PEARL HARBOR, HI 96860

COMMANDER NAVAL AIR FORCE
U.S. ATLANTIC FLEET (30F)
ATTN: NSAP SCIENCE ADVISOR
NORFOLK, VA 23511

COMNAVAIRPAC
ATTN: NSAP SCI. ADV. (016)
NAS, NORTH ISLAND
SAN DIEGO, CA 92135

COMNAVSURFLANT
ATTN: NSAP SCI. ADV. (N009)
NORFOLK, VA 23511

COMNAVSURFPAC
(005/N6N)
ATTN: NSAP SCIENCE ADVISOR
SAN DIEGO, CA 92155

COMMANDER
OPTEVFOR
ATTN: NSAP SCIENCE ADVISOR
NORFOLK, VA 23511

SPECIAL ASST. TO THE ASST.
SECRETARY OF THE NAVY (R&D)
ROOM 4E741, THE PENTAGON
WASHINGTON, DC 20350

CHIEF OF NAVAL OPERATIONS
(OP-952)
U.S. NAVAL OBSERVATORY
WASHINGTON, DC 20390

CHIEF OF NAVAL OPERATIONS
NAVY DEPT. OP-986G
WASHINGTON, DC 20350

OFFICE OF NAVAL TECHNOLOGY
MAT-0724, NAVY DEPT.
800 N. QUINCY ST.
ARLINGTON, VA 22217

DIRECTOR
DEFENSE NUCLEAR AGENCY
WASHINGTON, DC 20305

NAVAL DEPUTY TO THE
ADMINISTRATOR, NOAA
ROOM 200, PAGE BLDG. #1
3300 WHITEHAVEN ST. NW
WASHINGTON, DC 20235

OFFICER IN CHARGE
NAVOCEANCOMDET
AFGWC
OFFUTT AFB, NE 68113

COMMANDER
NAVAL OCEANOGRAPHY COMMAND
NSTL, MS 39529

COMMANDING OFFICER
NAVPOlarOCEANCEN
NAVY DEPT.
4301 SUITLAND RD.
WASHINGTON, DC 20390

COMMANDING OFFICER
U.S. NAVOCEANCOMCEN
BOX 31 (ROTA)
FPO NEW YORK 09540

NAVAL POSTGRADUATE SCHOOL
METEOROLOGY DEPT.
MONTEREY, CA 93943

COMMANDER (2)
NAVAIRSYSCOM
ATTN: LIBRARY (AIR-7226)
WASHINGTON, DC 20361

COMMANDER
NAVAIRSYSCOM (AIR-330)
WASHINGTON, DC 20361

COMMANDER
NAVAIRSYSCOM
MET. SYS. DIV. (AIR-553)
WASHINGTON, DC 20360

COMMANDER
NAVAL SEA SYSTEMS COMMAND
ATTN: LCDR S. GRIGSBY
PMS-405/PM-22
WASHINGTON, DC 20362

COMMANDER
NAVOCEANSYSCEN
DR. J. RICHTER, CODE 532
SAN DIEGO, CA 92152

COMMANDER
NAVAL SURFACE WEAPONS CENTER
DAHLGREN, VA 22448

COMMANDER
NAVSURFWEACEN, CODE R42
DR. B. KATZ, WHITE OAKS LAB
SILVER SPRING, MD 20910

COMMANDER
NAVAL SURFACE WEAPONS CENTER
ATTN: CODE 44
DAHLGREN, VA 22448

NAVAL SPACE SYSTEMS ACTIVITY
CODE 60
P.O. BOX 92960
WORLDWAY POSTAL CENTER
LOS ANGELES, CA 90009

COMMANDER
PACMISTESTCEN
GEOPHYSICS OFFICER
PT. MUGU, CA 93042

USAFETAC/TS
SCOTT AFB, IL 62225

AFGL/LY
HANSCOM AFB, MA 01731

5WW/DN
LANGLEY AFB, VA 23665

OFFICE OF STAFF METEOROLOGY
WESTERN SPACE & MISSILE
CENTER (WE)
VANDENBERG AFB, CA 93437

OFFICER IN CHARGE
SERVICE SCHOOL COMMAND
DET. CHANUTE/STOP 62
CHANUTE AFB, IL 61868

COMMANDER & DIRECTOR
ATTN: DELAS-D
U.S. ARMY ATMOS. SCI. LAB
WHITE SANDS MISSILE RANGE
WHITE SANDS, NM 88002

DIRECTOR (12)
DEFENSE TECH. INFORMATION
CENTER, CAMERON STATION
ALEXANDRIA, VA 22314

DIRECTOR, SYSTEMS DEVELOPMENT
NWS, NOAA
RM 1216 - THE GRAMAX BLDG.
8060 13TH ST.
SILVER SPRING, MD 20910

DIRECTOR
NATIONAL METEORO. CENTER
NWS, NOAA
WWB W32, RM 204
WASHINGTON, DC 20233

DIRECTOR
NATIONAL EARTH SAT. SERV/SEL
FB-4, S321B
SUITLAND, MD 20233

DIRECTOR
NATIONAL SEVERE STORMS LAB
1313 HALLEY CIRCLE
NORMAN, OK 73069

DIRECTOR
PACIFIC MARINE CENTER
NATIONAL OCEAN SURVEY, NOAA
1801 FAIRVIEW AVE., EAST
SEATTLE, WA 98102

NOAA-NESDIS LIAISON, CODE SC2
NASA-JOHNSON SPACE CENTER
HOUSTON, TX

METEOROLOGIST IN CHARGE
WEA. SERV. FCST. OFFICE, NOAA
660 PRICE AVE.
REDWOOD CITY, CA 94063

CHIEF
MESOSCALE APPLICATIONS BRANCH
NATIONAL EARTH SAT. SERV.
1225 W. DAYTON
MADISON, WI 53562

MANAGER
NATIONAL EARTH SAT.SERV.
SATELLITE FIELD SERV. STN.
701 C ST., BOX 45
ANCHORAGE, AK 99513

DIRECTOR
TECHNIQUES DEVELOPMENT LAB
GRAMAX BLDG.
8060 13TH ST.
SILVER SPRING, MD 20910

HEAD, ATMOS. SCIENCES DIV.
NATIONAL SCIENCE FOUNDATION
1800 G STREET, NW
WASHINGTON, DC 20550

COLORADO STATE UNIVERSITY
ATMOSPHERIC SCIENCES DEPT.
ATTN: DR. WILLIAM GRAY
FORT COLLINS, CO 80523

CHAIRMAN, METEOROLOGY DEPT.
CALIFORNIA STATE UNIVERSITY
SAN JOSE, CA 95192

COLORADO STATE UNIVERSITY
ATMOSPHERIC SCIENCES DEPT.
ATTN: LIBRARIAN
FT. COLLINS, CO 80523

CHAIRMAN, METEOROLOGY DEPT.
METEORO. & SPACE SCI. BLDG.
1225 W. DAYTON ST.
MADISON, WI 53706

UNIVERSITY OF WASHINGTON
ATMOSPHERIC SCIENCES DEPT.
SEATTLE, WA 98195

DIRECTOR, REMOTE SENSING LAB
UNIVERSITY OF MIAMI
P.O. BOX 248003
CORAL GABLES, FL 33124

CHAIRMAN, METEOROLOGY DEPT.
PENNSYLVANIA STATE UNIV.
503 DEIKE BLDG.
UNIVERSITY PARK, PA 16802

CHAIRMAN
METEOROLOGY DEPT.
MASSACHUSETTS INSTITUTE OF
TECHNOLOGY
CAMBRIDGE, MA 02139

CHAIRMAN, METEOROLOGY DEPT.
UNIVERSITY OF UTAH
SALT LAKE CITY, UT 84112

SCIENCE APPLICATIONS, INC.
2999 MONTEREY-SALINAS HWY.
MONTEREY, CA 93940

MR. W. G. SCHRAMM/WWW
WORLD METEOROLOGICAL
ORGANIZATION
CASE POSTALE #5, CH-1211
GENEVA, SWITZERLAND

LIBRARIAN, METEOROLOGY DEPT.
UNIVERSITY OF MELBOURNE
PARKVILLE, VICTORIA 3052
AUSTRALIA

BUREAU OF METEOROLOGY
BOX 1289K, GPO
MELBOURNE, VIC, 3001
AUSTRALIA

INSTITUTE OF OCEANOGRAPHY
UNIV. OF BRITISH COLUMBIA
VANCOUVER BC, CANADA V6T-1W5

EUROPEAN CENTRE FOR MEDIUM
RANGE WEATHER FORECASTS
SHINFIELD PARK, READING
BERKSHIRE RG29AX, ENGLAND

EUROPEAN SPACE OPERATIONS
ATTN: DR. J. MORGAN, METEO.
SAT. DATA, MANAGEMENT DEPT.
R. BOSCH STR 5 D61 DARMSTADT
FEDERAL REPUBLIC OF GERMANY

HEAD, DATA PROCESSING SEC.
GERMAN MILITARY GEOPHYS.
MONT-ROYAL, D5580
TRAVEN-TRARBACH
FEDERAL REPUBLIC OF GERMANY

4-10-68

FILED